Numerical stability for velocity-based 2-phase formulation for geotechnical dynamic analysis

August 16, 2015

M.M.J. Mieremet

Technische Universiteit Delft

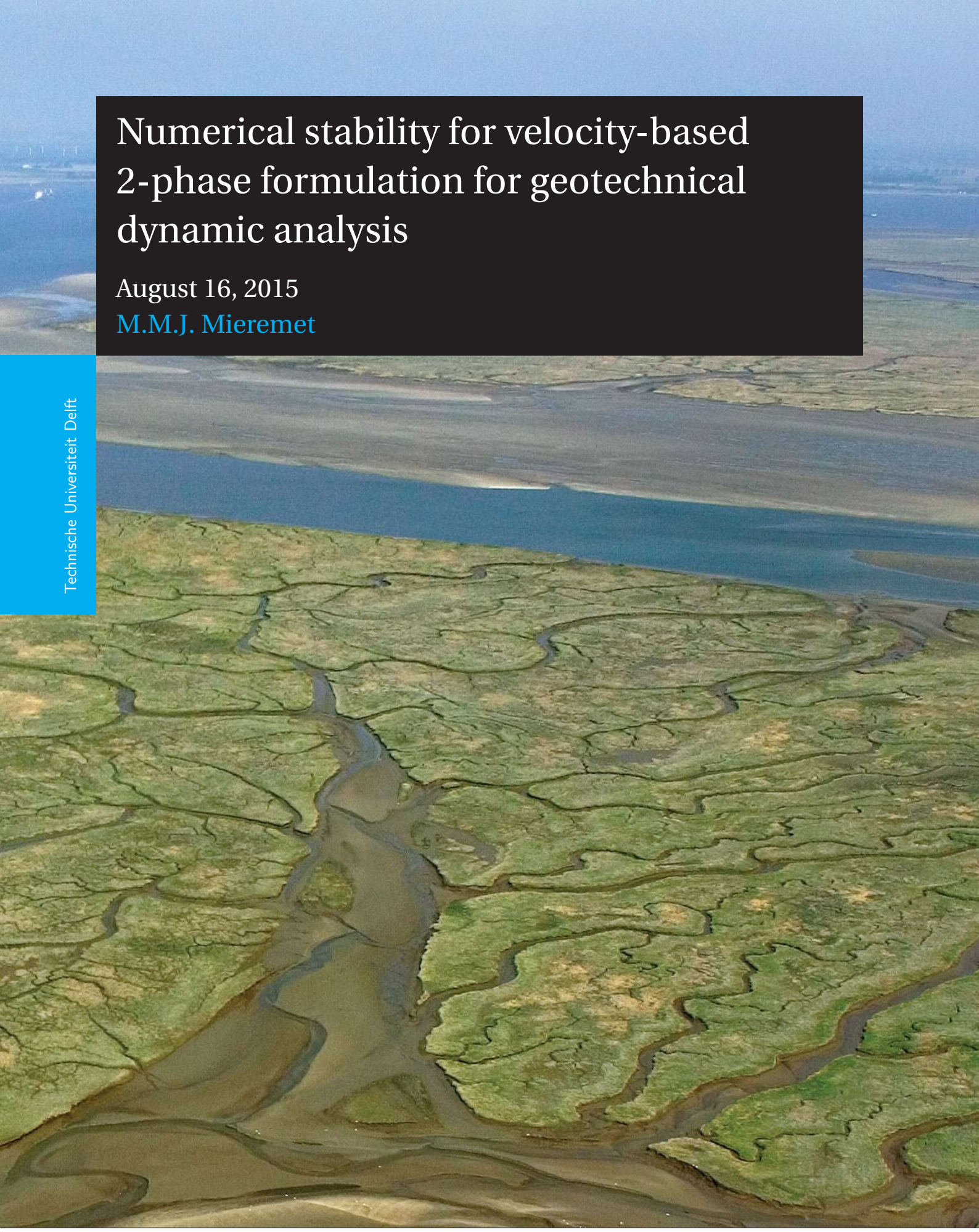

TU Delft Delft University of Technology

Deltares Enabling Delta Life

Challenge the future

NUMERICAL STABILITY FOR VELOCITY-BASED 2-PHASE FORMULATION FOR GEOTECHNICAL DYNAMIC ANALYSIS

AUGUST 16, 2015

by

M.M.J. Mieremet

in partial fulfillment of the requirements for the degree of

Master of Science
in Applied Mathematics

at the Delft University of Technology
to be defended publicly on Friday August 28, 2015 at 02:00 PM.

Supervisors:	Prof.dr.ir. C. Vuik	TU Delft
	Dr.-Ing. L.I. Beuth	Deltares
Thesis commitee:	Dr. H.M. Schuttelaars	TU Delft
	Prof.dr. D.F. Stolle	McMaster University

TU Delft Delft University of Technology

Deltares Enabling Delta Life

PREFACE

The master thesis in front of you is the result of a challenging study in the field of geotechnical engineering and numerical analysis. By means of an internship at Deltares, I have been able to gain insight into the modelling of soil, apply my knowledge of the finite element method and learn all about the material point method. Last but not least, I was allowed to travel to Germany and Spain to present my findings in front of other researchers. It was an experience I will not soon forget.

The opportunities that I was given during the last year were incredibly instructive and were only possible because of the support of Deltares and my daily supervisor Lars Beuth. Also the trust and effort of Cees Vuik, professor in Numerical Analysis, and Dieter Stolle, professor in Geotechnical Engineering, were very important to me. Finally, I would like to acknowledge the help and advice of Francesca Ceccato. We only met in the early stage of this study, but she voluntary kept in touch throughout the full time line.

I would also like to express sincere gratitude to my direct colleagues of the GEO department for the great time at Deltares. I very much enjoyed the lunch breaks, the apple pie meetings and all other activities.

In my personal life I would like to thank René Mieremet, Marij Mieremet-Ooms and Joost Klip for their endless love. It gave me the courage to continue, even in difficult times. I also owe to Wil van Marrewijk and Julie Le Grand for helping me to grow in personal development.

M.M.J. Mieremet
Delft, August 2015

CONTENTS

1

INTRODUCTION

A basic problem in geotechnical engineering is to predict the deformation of soil upon arbitrary loading, taking into account its highly non-linear mechanical behaviour. Since soil is a porous medium, commonly saturated with water, deformation analyses often require to consider soil as a 2-phase material. Extensive research is being done to develop accurate physical models, for instance for analyzing dike safety [1, 2] or studying pile installation [3].
It should be noted that physical models used for these and other 2-phase problems are also applicable in other disciplines involving porous media, such as biomechanics [4, 5] or acoustical physics [6] and thus of even broader value.

New developments in numerical analysis render new opportunities for application of these physical models. The widely-used finite element method (FEM) is capable of handling problems involving complex geometries. While FEM is limited to small to moderately large deformations, the relatively new material point method (MPM) opens the path to solving problems involving arbitrary large deformations of soil or other solid materials.

At Deltares, a Dutch research and consulting institute, a 2-phase MPM is being developed for geotechnical applications together with partners[1] in the frame of a research community. The MPM is being used in challenging simulations of slope failures, cone penetration testing and the installation of piles.

Numerical stability issues have appeared with this 2-phase MPM [7], especially concerning saturated soil with a low permeability. Owing to the used semi-implicit and conditionally stable time integration scheme, a criterion is required for limiting the size of time steps in which a simulation is advanced in time to ensure numerical stability. The initially used Courant-Friedrich-Lewy (CFL) condition for undrained wave propagation [8], however, proved to be unreliable. Calculations such as those listed above generally take a lot of computational time. It is therefore of high importance to obtain not only a reliable, but also an efficient time step criterion.

In the preliminary study of this thesis [9] a permeability-dependent criterion was obtained through study of a simplified problem assuming an incompressible pore fluid. However, the combination of the CFL condition and this permeability-dependent criterion still proved to be insufficient to garantee numerical stability of the 2-phase MPM.

The 2-phase formulation assuming a compressible pore fluid, used with the MPM, has been analyzed in the final study of this thesis. Since MPM can be considered as an extension of FEM, a stability criterion found with the FEM can be used with MPM, too. Because the numerical stability analysis is easier with FEM than MPM, the former is mainly considered here. Some statements on the stability of the 2-phase MPM are provided though at the end of this thesis.

[1] The universities of Cambridge, Hamburg, Barcelona, Padova and Delft, see www.mpm-dredge.eu.

This thesis is structured in the following way. First, a brief history on physical and numerical modelling of dynamic deformation analysis of soil is provided in Chapter 2. Then, the 2-phase formulation for saturated soil is explained in Chapter 3, followed by the finite element and time discretization in Chapter 4. The latter includes two benchmarks for validation of a Matlab implementation. A sufficient and efficient stability criterion is derived in Chapter 5. The material point method is explained in Chapter 6, as well as the application of the obtained stability criteria to it. Finally, concluding remarks and recommendations are presented in Chapter 7.

2

DYNAMIC DEFORMATION ANALYSIS OF SOIL

The simulation of deformation of soil forms a challenging task, but a lot of progress has been made in order to obtain accurate predictions. This chapter provides a breif overview of the developments that have been made during the last century with respect to both physical modelling in Section 2.1 and numerical modelling in Section 2.2.

2.1. PHYSICAL MODELLING

In geomechanics, soil is commonly modelled as a homogeneous continuum even though it consists of discrete solid grains, i.e. sand or clay particles, and pore volume filled with water and/or air. On a microscopic scale this modelling approach does not apply, but considering dimensions generally encountered in engineering practice it represents a reasonable approximation.

In the very beginning, soil was generally modelled as a 1-phase solid continuum, i.e. by neglecting the water flow through the pores. Depending on the degree of saturation and the loading velocity, fully drained or fully undrained situations could be modelled with this simplified approach. The stiffness properties of the continuum would be adapted with respect to the stiffness of the pore water in case of undrained conditions. For these two cases, a 1-phase formulation appears to be appropriate.
In 1925, Terzaghi [10] presented his model of one-dimensional consolidation, the generation of excess pore water pressures due to loading and subsequent gradual dissipation. Biot [11] extended this theory to three dimensions, which eventually resulted in 2-phase formulations used in numerical methods for modelling the deformation of saturated soil in a wide range of drainage conditions. Various 2-phase formulations can be found in e.g. Zienkiewicz et al. [12].
Recently, 3-phase formulations were developed to model the deformation of unsaturated soil, see e.g. Xikui and Zienkiewicz [13] and Yerro et al. [14]. These formulations capture the interaction between all three phases, i.e. soil, water and air.

Besides the study of consolidation, the highly non-linear relation between loading of soil and its deformation gained much scientific interest as well. Intensive research shows that the stiffness of soil depends on the stress history. Irreversible (plastic) deformation generally occurs.
The simplest models assuming elastic behaviour, either linear or non-linear, are therefore not very realistic. A perfect plasticity model which assumes a plastic yield stress independent of the stress level appeared to be more accurate. The Tresca model is for example used for cohesive soils like clay. The Mohr-Coulomb model is widely used for frictional material like sand.
One example of a more advanced model that takes into account a stress-dependent yield strength is the (modified) cam-clay model. However, it should be noted that more advanced models generally require a large number of parameters.
For the presented study, consideration of a linear elastic stress-strain relation is sufficient. The reader is referred to Yu [15] for more information on constitutive modelling.

2.2. NUMERICAL MODELLING

Applying numerical analysis to geotechnical problems involving a complex system of partial differential equations often requires discretization in both space and time. Here, spatial derivatives are firstly approximated through a spatial discretization method and the resulting system of ordinary differential equations is numerically solved with some time-stepping scheme. Since each discretization method has its own advantages and disadvantages, this section will give a brief overview of the developments in numerical methods used for geotechnical problems.

Before the introduction of the computer to solve differential equations, approximate solutions were obtained using for example Lagrangian interpolation functions, Gaussian integration and Euler's method. Nowadays a multitude of numerical methods have taken over the task; e.g. the finite difference method (FDM), finite volume method (FVM) and finite element method (FEM), see Van Kan et al. [16].

Van Kan mentions that FEM is well suited for unstructured grids. Also the easy way of constructing the required matrices and the natural way of handling boundary conditions makes FEM preferable over FDM and FVM. The Lagrangian finite element description also provides the possibility to trace the loading history at the material coordinates. Various engineering problems, including dynamic geotechnical problems discussed in this thesis, require such treatment. It is therefore not surprising that FEM quickly became popular after its introduction in the mid 20th century.
For large deformation problems it is necessary to switch to the updated Lagrangian FEM, where stresses are calculated according to the updated configuration. There is however one drawback with large deformation problems that could not be solved: elements can get heavily distorted such that accuracy is reduced.

With the need for a numerical method to solve geotechnical problems without the drawback of element distortions, Sulsky et al. [17] introduced the material point method (MPM) in 1994. This method uses a cloud of so-called material points that flow through a background finite element mesh. Therefore, MPM is often considered as an extension of FEM. The method preserves the advantages of FEM, while it overcomes the problematic element distortion.

In addition to the developments related to space discretization, time stepping schemes also received much attention. Clearly, implicit schemes would be preferable over explicit schemes because they are unconditionally stable. However, they require iterative multiplication or inverse calculation of large matrices, which is time-consuming. Within the context of explicit time stepping algorithms, the semi-implicit Euler-Cromer method [18] is a popular choice. This scheme is computationally inexpensive, conditionally stable and first order accurate like the often used Euler Forward scheme, but is energy conservative while the Euler Forward scheme is not. Nowadays, the Euler-Cromer method is widely used in FEM- and MPM-calculations of geotechnical problems, although there is still research on the possibility to use implicit schemes [19, 20].

3

PHYSICAL MODEL

In this thesis the velocity-based 2-phase formulation of Van Esch et al. [21] is considered to model dynamic deformation of saturated soil. Here, soil is considered to be a homogeneous and isotropic 2-phase continuum. Its deformation is described in terms of the velocities of the solid and fluid, respectively.

This chapter provides the physical model for one-dimensional deformation. The physical model for three-dimensional deformation will not be used in this thesis, but is added in Appendix A for completeness. The theory will be presented in terms of soil and water, but can be easily applied to other materials, i.e. porous media filled with a liquid in general.

The chapter begins by defining the relevant variables in Section 3.1. Then, the partial differential equations that describe the deformation of saturated soil are presented in Sections 3.2, 3.3 and 3.4. They are derived from the conservation of mass, the conservation of momentum and the constitutive relation of soil, respectively. Finally, initial and boundary conditions are described in Section 3.5.

3.1. DEFINITION OF VARIABLES

Soil is a granular material filled with water and/or air, see Figure 3.1. The total volume V is composed of the volume of the solid grains V_s, the volume of the water V_w and the volume of the air V_a. The void volume V_v is the sum of the volume of water and air.

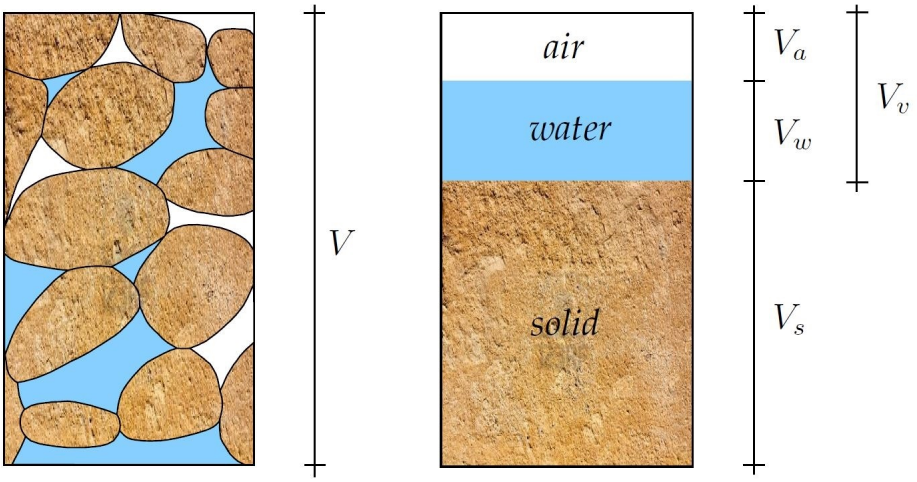

Figure 3.1: Constituents of soil: solid grains, water and air [22]

The ratio between the void volume and the total volume is expressed through the porosity

$$n = \frac{V_v}{V}, \tag{3.1}$$

and the ratio between the water volume and the void volume through the degree of saturation

$$S_r = \frac{V_w}{V_v} \times 100\%. \tag{3.2}$$

In this thesis only fully saturated soil is considered, i.e. $S_r = 100\%$.

When the densities of the solid grains and water are represented by ρ_s and ρ_w, respectively, the saturated soil then has density

$$\rho_{sat} = (1-n)\rho_s + n\rho_w. \tag{3.3}$$

Since spatial dimensions of problems encountered in engineering practice are generally on a macroscopic level, modelling the soil as a 2-phase continuum is reasonable. The continuum is assumed to be homogeneous and isotropic, which means that all material properties are equal at any material point in any direction.

As a consequence of modelling soil as a continuum, all variables are considered to be a continuous function of space and time. Since the formulation is defined in a Lagrangian framework, the material coordinate x_0 is used as well as partial rather than material time derivatives. Consequently, the displacement and velocity of the solid phase are given by

$$\hat{u}_s(x_0,t) \quad \text{and} \quad \hat{v}_s(x_0,t) = \frac{\partial \hat{u}_s}{\partial t}(x_0,t). \tag{3.4}$$

Similarly, the displacement u_w and velocity v_w of the water phase are given by

$$\hat{u}_w(x_0,t) \quad \text{and} \quad \hat{v}_w(x_0,t) = \frac{\partial \hat{u}_w}{\partial t}(x_0,t). \tag{3.5}$$

It should be noted that the relative motion of water and soil, i.e. the displacement of pore water, is not traced with the formulation. This variable is only introduced because of its use in the stability analysis in Chapter 5.

The effective stress of the soil and the pore pressure of the water are represented by scalar functions

$$\hat{\sigma}'(x_0,t) \quad \text{and} \quad \hat{p}(x_0,t), \tag{3.6}$$

respectively. According to the principle of effective stress by Terzaghi [10], the effective stress and the pore pressure compose the total stress

$$\hat{\sigma}(x_0,t) = \hat{\sigma}'(x_0,t) + \hat{p}(x_0,t). \tag{3.7}$$

Here, stress and pressure are defined to be positive in tension, suction respectively. It is assumed that the effective stress remains negative, which corresponds to the assumption of solid grains remaining in contact. If the solid grains do not form a soil skeleton, the deformation is governed by different mechanical processes, not considered in this thesis.

3.2. CONSERVATION OF MASS

Mass is a conservative quantity and both soil and water need to satisfy the corresponding continuity equation. This differential equation links the amount of the conserved quantity, i.e. mass, to the transport of that quantity.

The conservation of mass of the soil is expressed as

$$\frac{\partial}{\partial t}\left[(1-n)\rho_s\right] + \frac{\partial}{\partial x_0}\left[(1-n)\rho_s \hat{v}_s\right] = 0. \tag{3.8}$$

Similarly, the conservation of mass of the water is expressed as

$$\frac{\partial}{\partial t}\left[n\rho_w\right] + \frac{\partial}{\partial x_0}\left[n\rho_w \hat{v}_w\right] = 0. \tag{3.9}$$

It is assumed that the soil is incompressible and the water is linearly compressible, yielding

$$\frac{\partial \rho_s}{\partial t} = 0 \quad \text{and} \quad \frac{\partial \rho_w}{\partial \hat{p}} = -\frac{\rho_w}{K_w}, \tag{3.10}$$

with K_w being the bulk modulus of water. When neglecting a spatial variation in density and porosity, we can reduce Equation 3.8 and 3.9 to

$$-\rho_s \frac{\partial n}{\partial t} + (1-n)\rho_s \frac{\partial \hat{v}_s}{\partial x_0} = 0, \tag{3.11}$$

and

$$-n\frac{\rho_w}{K_w}\frac{\partial \hat{p}}{\partial t} + \rho_w \frac{\partial n}{\partial t} + n\rho_w \frac{\partial \hat{v}_w}{\partial x_0} = 0. \tag{3.12}$$

Elimination of the term $\frac{\partial n}{\partial t}$ results in

$$\frac{\partial \hat{p}}{\partial t} = \frac{K_w}{n}\left[(1-n)\frac{\partial \hat{v}_s}{\partial x_0} + n\frac{\partial \hat{v}_w}{\partial x_0}\right], \tag{3.13}$$

which is known as the storage equation.

3.3. CONSERVATION OF MOMENTUM

Momentum is the second conserved quantity that is considered. We can distinguish linear and angular momentum, but the latter is zero with one-dimensional deformation. Therefore, we will only look at the equations that belong to the conservation of linear momentum.

From Newton's laws of motion [23] we know that the rate of change of linear momentum of a particle is equal to the force(s) acting on it. We consider internal forces, a gravitational force and a coupling term acting as a drag force.

Taking into account the above-mentioned forces, the conservation of momentum of soil is given by

$$(1-n)\rho_s \frac{\partial \hat{v}_s}{\partial t} = \frac{\partial \hat{\sigma}'}{\partial x_0} + (1-n)\frac{\partial \hat{p}}{\partial x_0} - (1-n)\rho_s g + \frac{n^2 \rho_w g}{k}(\hat{v}_w - \hat{v}_s), \tag{3.14}$$

with g being the gravitational acceleration and k the hydraulic conductivity of the soil, also known as the Darcy permeability. The term $\hat{v}_w - \hat{v}_s$ represents the relative velocity between both media.

The conservation of momentum of water is given by

$$n\rho_w \frac{\partial \hat{v}_w}{\partial t} = n\frac{\partial \hat{p}}{\partial x_0} - n\rho_w g - \frac{n^2 \rho_w g}{k}(\hat{v}_w - \hat{v}_s). \tag{3.15}$$

Adding Equation 3.14 and 3.15 yields the equation for conservation of linear momentum of the soil-water mixture, i.e. the saturated soil,

$$(1-n)\rho_s \frac{\partial \hat{v}_s}{\partial t} + n\rho_w \frac{\partial \hat{v}_w}{\partial t} = \frac{\partial \hat{\sigma}'}{\partial x_0} + \frac{\partial \hat{p}}{\partial x_0} - \rho_{sat} g. \tag{3.16}$$

The momentum equations for the water and for the mixture, i.e. Equation 3.15 and 3.16, form the two equations of motion that are solved with the considered 2-phase formulation for velocities $\hat{v}_s$ and $\hat{v}_w$.

3.4. CONSTITUTIVE RELATION

Finally, the effective stress of the soil is related to its deformations. As mentioned in Chapter 2, various constitutive relations might be considered, most of which are non-linear. Since stability analysis methods require linear equations, non-linear relations need to be linearized. For simplicity, a linear constitutive relation is assumed in this thesis.

The stress rate of a linear-elastic material is given by

$$\frac{\partial \hat{\sigma}'}{\partial t} = E^c \frac{\partial \hat{\epsilon}}{\partial t}, \tag{3.17}$$

with strain rate

$$\frac{\partial \hat{\epsilon}}{\partial t} = \frac{\partial \hat{v}_s}{\partial x_0} \tag{3.18}$$

and constrained modulus

$$E^c = \frac{(1-\nu)E}{(1+\nu)(1-2\nu)}. \tag{3.19}$$

The latter one depends on material parameters being Young's modulus E and Poisson ratio ν.

Equation 3.17 together with Equation 3.13, 3.15 and 3.16 are used to compute the unknown phase velocities, effective stress and pore pressure with the velocity-based 2-phase formulation.

3.5. INITIAL AND BOUNDARY CONDITIONS

The four equations considered form a system of coupled partial differential equations that should be satisfied in a certain domain Ω and time interval $t > 0$. In order to obtain a unique solution, one boundary condition is required for each phase at each point of the boundary as well as one initial condition for each variable.

Both Dirichlet and Neumann boundary conditions are considered. For the soil phase this results in a prescribed velocity boundary and a prescribed total stress boundary. It should be noted that they do not intersect, while their union covers the whole boundary. For the water phase we distinguish between a prescribed velocity boundary and a prescribed pressure boundary, with the same intersection and union criteria.

In this thesis, a column of height H is considered as a benchmark, such that the domain is given by $\Omega = [0, H]$. The bottom at $x_0 = 0$ is assumed to be fixed, implying homogeneous prescribed velocity boundary conditions for both soil and water. At the top of the column a constant load is applied, implying a prescribed total traction boundary condition for soil and a prescribed pressure boundary condition for water.

The velocity boundary conditions are written as

$$\hat{v}_s(0,t) = 0, \tag{3.20}$$
$$\hat{v}_w(0,t) = 0. \tag{3.21}$$

The total traction and pressure boundary conditions are written as

$$\hat{\sigma}(H,t) = \bar{\sigma}, \tag{3.22}$$
$$\hat{p}(H,t) = \bar{p}. \tag{3.23}$$

The required initial conditions equal

$$\hat{v}_s(x_0,0) = \hat{v}_{s,0}(x_0), \tag{3.24}$$
$$\hat{v}_w(x_0,0) = \hat{v}_{w,0}(x_0), \tag{3.25}$$
$$\hat{\sigma}'(x_0,0) = \hat{\sigma}'_0(x_0), \tag{3.26}$$
$$\hat{p}(x_0,0) = \hat{p}_0(x_0). \tag{3.27}$$

It should be noted that throughout this thesis the boundary conditions can be recognized by the bar and the initial conditions by the subscript $(\cdot)_0$.

4

NUMERICAL MODEL

The velocity-based 2-phase formulation is a system of coupled partial differential equations. It is generally difficult to solve such a system analytically for typical problems in geotechnical engineering. The finite element method (FEM) is an attractive method to solve the equations numerically provided deformations of the soil remain small. Otherwise, enhanced methods such as the updated Lagrangian FEM (UL-FEM) or material point method (MPM) might be used.

This chapter presents the numerical solution to the equations of the 2-phase formulation that are introduced in Chapter 3 using FEM. First, the finite element space discretization is considered in Section 4.1. Subsequently, the Euler-Cromer time discretization is presented in Section 4.2. Finally, a Matlab implementation is validated in Section 4.3. The validation is done by means of two benchmarks, one-dimensional wave propagation and one-dimensional consolidation.

4.1. FINITE ELEMENT METHOD

The finite element method is a spatial discretization method where the exact solution of differential equations across a spatial domain is approximated from discrete values by a linear combination of shape functions. The discrete values are computed at nodes of a grid laid across the considered spatial domain. The introduction of this approximation to the system of coupled partial differential equations of the 2-phase formulation results in a system of ordinary differential equations.

In this section, this system of ordinary differential equations is stepwise derived. First, the weak form of the momentum equations is obtained. Then, the discretization with shape functions is introduced. Finally, the system of ordinary differential equations is derived.

WEAK FORM OF MOMENTUM EQUATIONS

The starting point of the derivation are the momentum equations of the water and the soil-water mixture, repeated here

$$n\rho_w \frac{\partial \hat{v}_w}{\partial t} = n\frac{\partial \hat{p}}{\partial x_0} - n\rho_w g - \frac{n^2 \rho_w g}{k}(\hat{v}_w - \hat{v}_s), \tag{4.1}$$

$$(1-n)\rho_s \frac{\partial \hat{v}_s}{\partial t} + n\rho_w \frac{\partial \hat{v}_w}{\partial t} = \frac{\partial \hat{\sigma}'}{\partial x_0} + \frac{\partial \hat{p}}{\partial x_0} - \rho_{sat} g. \tag{4.2}$$

It should be noted that Equation 4.1 can be simplified through division by porosity n.

The weak forms of Equation 4.1 and 4.2 are obtained by multiplication with virtual velocities $\partial\hat{v}_s$ and $\partial\hat{v}_w$, and integration over the domain $\Omega = [0, H]$

$$\int_0^H \delta\hat{v}_w \rho_w \frac{\partial \hat{v}_w}{\partial t} dx_0 = \int_0^H \delta\hat{v}_w \frac{\partial \hat{p}}{\partial x_0} dx_0 - \int_0^H \delta\hat{v}_w \rho_w g dx_0 - \int_0^H \delta\hat{v}_w \frac{n\rho_w g}{k}(\hat{v}_w - \hat{v}_s) dx_0, \tag{4.3}$$

$$\int_0^H \delta\hat{v}_s (1-n)\rho_s \frac{\partial \hat{v}_s}{\partial t} dx_0 + \int_0^H \delta\hat{v}_s n\rho_w \frac{\partial \hat{v}_w}{\partial t} dx_0 = \int_0^H \delta\hat{v}_s \left(\frac{\partial \hat{\sigma}'}{\partial x_0} + \frac{\partial \hat{p}}{\partial x_0}\right) dx_0 - \int_0^H \delta\hat{v}_s \rho_{sat} g dx_0. \tag{4.4}$$

Integration by parts introduces the boundary conditions in a natural way. The virtual velocities $\delta\hat{v}_s$ and $\delta\hat{v}_w$ vanish wherever the velocities $\hat{v}_s$ and $\hat{v}_w$ are prescribed. We obtain

$$\int_0^H \delta\hat{v}_w \rho_w \frac{\partial \hat{v}_w}{\partial t} dx_0 = \delta\hat{v}_w \bar{p}\Big|_H - \int_0^H \frac{\partial \delta\hat{v}_w}{\partial x_0} \hat{p} dx_0 - \int_0^H \delta\hat{v}_w \rho_w g dx_0 - \int_0^H \delta\hat{v}_w \frac{n\rho_w g}{k}(\hat{v}_w - \hat{v}_s) dx_0, \tag{4.5}$$

$$\int_0^H \delta\hat{v}_s (1-n)\rho_s \frac{\partial \hat{v}_s}{\partial t} dx_0 + \int_0^H \delta\hat{v}_s n\rho_w \frac{\partial \hat{v}_w}{\partial t} dx_0 = \delta\hat{v}_s \bar{\sigma}\Big|_H - \int_0^H \frac{\partial \delta\hat{v}_s}{\partial x_0} (\hat{\sigma}' + \hat{p}) dx_0 - \int_0^H \delta\hat{v}_s \rho_{sat} g dx_0. \tag{4.6}$$

Equation 4.5 and 4.6 are the weak forms of Equation 4.1 and 4.2, respectively. They are also referred to as the virtual work equations.

FINITE ELEMENT DISCRETIZATION

As mentioned before, the exact solution is approximated with the FEM by a linear combination of shape functions. The corresponding values are computed from solutions of the equations obtained at discrete points in space. These points, nodes, span a grid of finite elements that subdivide a domain. The order of the chosen shape functions determines the accuracy of the FEM. In this thesis only linear shape functions are considered, as it is relevant to the MPM code developed by Deltares and partners.

With linear shape functions, the one-dimensional domain $\Omega = [0, H]$ is discretized with 2-noded line elements. We consider n_e elements and $n_n = n_e + 1$ nodes, see Figure 4.1. For the stability analysis in Chapter 5 it is convenient to consider a uniform grid with grid size $\Delta x_0 = H/n_e$.

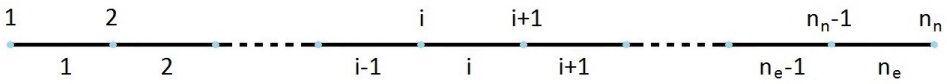

Figure 4.1: One-dimensional domain discretized with 2-noded linear elements [9]

The linear shape function belonging to node i is denoted by $N_i(x_0)$. This function is a continuous piecewise-linear function that is equal to 1 at node i and 0 at node $j \neq i$, see Figure 4.2.

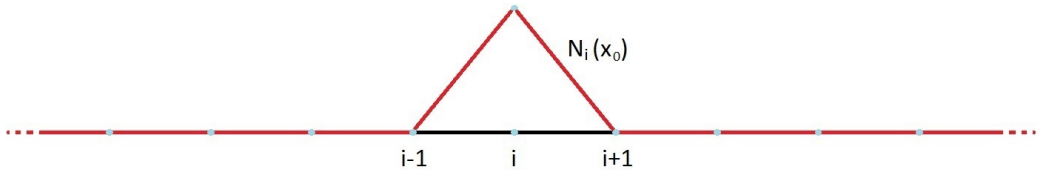

Figure 4.2: Linear shape function $N_i(x_0)$ [9]

Given the one-dimensional nature of the problem addressed in this thesis, the shape functions can be conveniently stored in a shape function vector $\mathbf{N}(x_0)$

$$\mathbf{N}(x_0) = \begin{bmatrix} N_1(x_0) & \cdots & N_{n_n}(x_0) \end{bmatrix}. \tag{4.7}$$

Now the displacement and (virtual) velocity functions can be approximated with a linear combination of the shape functions

$$\begin{aligned} \hat{u}_s(x_0,t) &\approx \mathbf{N}(x_0)\mathbf{u}_s(t), & \hat{v}_s(x_0,t) &\approx \mathbf{N}(x_0)\mathbf{v}_s(t), & \delta\hat{v}_s(x_0,t) &\approx \mathbf{N}(x_0)\delta\mathbf{v}_s(t), \\ \hat{u}_w(x_0,t) &\approx \mathbf{N}(x_0)\mathbf{u}_w(t), & \hat{v}_w(x_0,t) &\approx \mathbf{N}(x_0)\mathbf{v}_w(t), & \delta\hat{v}_w(x_0,t) &\approx \mathbf{N}(x_0)\delta\mathbf{v}_w(t). \end{aligned} \tag{4.8}$$

where the displacement and (virtual) velocity vectors represent the time-dependent nodal values

$$\begin{aligned} \mathbf{u}_s(t) &= \begin{bmatrix} u_{s,1}(t) \\ \vdots \\ u_{s,n_n}(t) \end{bmatrix}, & \mathbf{v}_s(t) &= \begin{bmatrix} v_{s,1}(t) \\ \vdots \\ v_{s,n_n}(t) \end{bmatrix}, & \delta\mathbf{v}_s(t) &= \begin{bmatrix} \delta v_{s,1}(t) \\ \vdots \\ \delta v_{s,n_n}(t) \end{bmatrix}, \\ \mathbf{u}_w(t) &= \begin{bmatrix} u_{w,1}(t) \\ \vdots \\ u_{w,n_n}(t) \end{bmatrix}, & \mathbf{v}_w(t) &= \begin{bmatrix} v_{w,1}(t) \\ \vdots \\ v_{w,n_n}(t) \end{bmatrix}, & \delta\mathbf{v}_w(t) &= \begin{bmatrix} \delta v_{w,1}(t) \\ \vdots \\ \delta v_{w,n_n}(t) \end{bmatrix}. \end{aligned} \tag{4.9}$$

The linear operator $\frac{\partial}{\partial x_0}$ is represented by L, such that the strain-displacement vector $\mathbf{B}(x_0)$ is given by

$$\mathbf{B}(x_0) = \begin{bmatrix} B_1(x_0) & \cdots & B_{n_n}(x_0) \end{bmatrix}, \tag{4.10}$$

with

$$B_i(x_0) = LN_i(x_0). \tag{4.11}$$

A different approach has to be taken with the effective stress and pore pressure. As a consequence of using linear shape functions for displacement and velocity, the effective stress and pore pressure are constant inside each element. Therefore, step functions $K_e(x_0)$ are introduced, which are equal to 1 in element e and 0 elsewhere in the domain, see Figure 4.3.

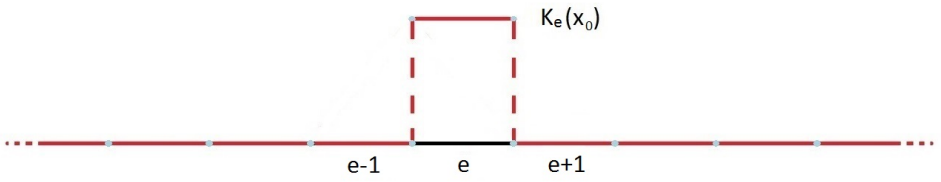

Figure 4.3: Step function $K_e(x_0)$ [9]

The step function vector $\mathbf{K}(x_0)$ contains all individual step functions

$$\mathbf{K}(x_0) = \begin{bmatrix} K_1(x_0) & \cdots & K_{n_e}(x_0) \end{bmatrix}. \tag{4.12}$$

The effective stress and pore pressure are then approximated by

$$\hat{\sigma}'(x_0,t) \approx \mathbf{K}(x_0)\boldsymbol{\sigma}'(t), \qquad \hat{p}(x_0,t) \approx \mathbf{K}(x_0)\mathbf{p}(t). \tag{4.13}$$

The vectors $\boldsymbol{\sigma}'(t)$ and $\mathbf{p}(t)$ store the computed values of the effective stress and pore pressure at integration points

$$\boldsymbol{\sigma}'(t) = \begin{bmatrix} \sigma'_1(t) \\ \vdots \\ \sigma'_{n_e}(t) \end{bmatrix}, \qquad \mathbf{p}(t) = \begin{bmatrix} p_1(t) \\ \vdots \\ p_{n_e}(t) \end{bmatrix}. \tag{4.14}$$

It should be noted that the integration points generally do not coincide with the locations of the nodes.

SYSTEM OF ORDINARY DIFFERENTIAL EQUATIONS

Recall the weak form of the momentum equations in Equations 4.5 and 4.6. Substitution of all variables by their approximations yields

$$\begin{aligned} \int_0^H (\mathbf{N}\delta\mathbf{v}_w)^T \rho_w \mathbf{N} \frac{d\mathbf{v}_w}{dt} dx_0 &= (\mathbf{N}(H)\delta\mathbf{v}_w)^T \bar{p} - \int_0^H (\mathbf{B}\delta\mathbf{v}_w)^T \mathbf{K}\mathbf{p} dx_0 \\ &\quad - \int_0^H (\mathbf{N}\delta\mathbf{v}_w)^T \rho_w g dx_0 - \int_0^H (\mathbf{N}\delta\mathbf{v}_w)^T \frac{n\rho_w g}{k} \mathbf{N}(\mathbf{v}_w - \mathbf{v}_s) dx_0, \end{aligned} \tag{4.15}$$

$$\begin{aligned} \int_0^H (\mathbf{N}\delta\mathbf{v}_s)^T (1-n)\rho_s \mathbf{N} \frac{d\mathbf{v}_s}{dt} dx_0 &= -\int_0^H (\mathbf{N}\delta\mathbf{v}_s)^T n\rho_w \mathbf{N} \frac{d\mathbf{v}_w}{dt} dx_0 + (\mathbf{N}(H)\delta\mathbf{v}_s)^T \bar{\sigma} \\ &\quad - \int_0^H (\mathbf{B}\delta\mathbf{v}_s)^T \mathbf{K}\left(\boldsymbol{\sigma}' + \mathbf{p}\right) dx_0 - \int_0^H (\mathbf{N}\delta\mathbf{v}_s)^T \rho_{sat} g dx_0. \end{aligned} \tag{4.16}$$

Given the arbitrariness of the virtual velocities, Equations 4.15 and 4.16 can be reduced to

$$\begin{aligned} \int_0^H \mathbf{N}^T \rho_w \mathbf{N} dx_0 \frac{d\mathbf{v}_w}{dt} &= \mathbf{N}^T(H)\bar{p} - \int_0^H \mathbf{B}^T \mathbf{K} dx_0 \mathbf{p} \\ &\quad - \int_0^H \mathbf{N}^T \rho_w g dx_0 - \int_0^H \mathbf{N}^T \frac{n\rho_w g}{k} \mathbf{N} dx_0 (\mathbf{v}_w - \mathbf{v}_s), \end{aligned} \tag{4.17}$$

$$\begin{aligned} \int_0^H \mathbf{N}^T (1-n)\rho_s \mathbf{N} dx_0 \frac{d\mathbf{v}_s}{dt} &= -\int_0^H \mathbf{N}^T n\rho_w \mathbf{N} dx_0 \frac{d\mathbf{v}_w}{dt} + \mathbf{N}^T(H)\bar{\sigma} \\ &\quad - \int_0^H \mathbf{B}^T \mathbf{K} dx_0 \left(\boldsymbol{\sigma}' + \mathbf{p}\right) - \int_0^H \mathbf{N}^T \rho_{sat} g dx_0. \end{aligned} \tag{4.18}$$

Equation 4.17 and 4.18 can be written in matrix notation as

$$\mathbf{M}_w \frac{d\mathbf{v}_w}{dt} = \mathbf{F}^{trac,w} - \mathbf{F}^{int,w} + \mathbf{F}^{grav,w} - \mathbf{F}^{drag,w}, \tag{4.19}$$

$$\mathbf{M}_s \frac{d\mathbf{v}_s}{dt} = -\bar{\mathbf{M}}_w \frac{d\mathbf{v}_w}{dt} + \mathbf{F}^{trac} - \mathbf{F}^{int} + \mathbf{F}^{grav}. \tag{4.20}$$

Equation 4.19 has mass matrix

$$\mathbf{M}_w = \int_0^H \mathbf{N}^T \rho_w \mathbf{N} dx_0, \tag{4.21}$$

and force vectors

$$\mathbf{F}^{trac,w} = \mathbf{N}^T(H)\bar{p}, \tag{4.22}$$

$$\mathbf{F}^{int,w} = \mathbf{K}^p \mathbf{p} \quad \text{with} \quad \mathbf{K}^p = \int_0^H \mathbf{B}^T \mathbf{K} dx_0, \tag{4.23}$$

$$\mathbf{F}^{grav,w} = -\int_0^H \mathbf{N}^T \rho_w g dx_0, \tag{4.24}$$

$$\mathbf{F}^{drag,w} = \mathbf{Q}(\mathbf{v}_w - \mathbf{v}_s) \quad \text{with} \quad \mathbf{Q} = \int_0^H \mathbf{N}^T \frac{n\rho_w g}{k} \mathbf{N} dx_0. \tag{4.25}$$

Equation 4.20 has mass matrices

$$\mathbf{M}_s = \int_0^H \mathbf{N}^T (1-n)\rho_s \mathbf{N} dx_0, \tag{4.26}$$

$$\bar{\mathbf{M}}_w = \int_0^H \mathbf{N}^T n\rho_w \mathbf{N} dx_0, \tag{4.27}$$

and force vectors

$$\mathbf{F}^{trac} = \mathbf{N}^T(H)\bar{\sigma}, \tag{4.28}$$

$$\mathbf{F}^{int} = \mathbf{K}^\sigma \left(\boldsymbol{\sigma}' + \mathbf{p}\right) \quad \text{with} \quad \mathbf{K}^\sigma = \int_0^H \mathbf{B}^T \mathbf{K} dx_0, \tag{4.29}$$

$$\mathbf{F}^{grav} = -\int_0^H \mathbf{N}^T \rho_{sat} g dx_0. \tag{4.30}$$

With the finite element method, (numerical) integration is conveniently performed over the finite elements. Here, the element shape function vector $\mathbf{N}_e$, element strain-displacement vector $\mathbf{B}_e$ and element step function vector $\mathbf{K}_e$ are used

$$\mathbf{N}_e = \begin{bmatrix} N_i & N_{i+1} \end{bmatrix}, \quad \mathbf{B}_e = \begin{bmatrix} B_i & B_{i+1} \end{bmatrix}, \quad \mathbf{K}_e = \begin{bmatrix} K_e \end{bmatrix}. \tag{4.31}$$

As an example we show integration of the element mass matrix $\mathbf{M}_{w,e}$ corresponding to the mass matrix in Equation 4.21

$$\mathbf{M}_{w,e} = \int_{x_i}^{x_{i+1}} \mathbf{N}_e^T \rho_w \mathbf{N}_e dx_0. \tag{4.32}$$

It is common to first perform a coordinate transformation from the global coordinate system $x_0 \in [x_i, x_{i+1}]$ to a local coordinate system $\xi \in [0,1]$, see Appendix B for a detailed description. For the element mass matrix $\mathbf{M}_{w,e}$ this yields

$$\mathbf{M}_{w,e} = \int_0^1 \mathbf{N}_e^T \rho_w \mathbf{N}_e \Delta x_0 d\xi. \tag{4.33}$$

Subsequently, Gaussian quadrature is applied to approximate the integrals numerically. One Gaussian integration point located in the middle of the line element is considered, such that integration of polynomials up to first order is exact, see Appendix C. When the subscript $(\cdot)_q$ denotes calculation at the Gauss point, we obtain

$$\mathbf{N}_{eq} = \begin{bmatrix} \frac{1}{2} & \frac{1}{2} \end{bmatrix}, \qquad \mathbf{B}_{eq} = \begin{bmatrix} -\frac{1}{\Delta x_0} & \frac{1}{\Delta x_0} \end{bmatrix}, \qquad \mathbf{K}_{eq} = \begin{bmatrix} 1 \end{bmatrix}. \tag{4.34}$$

The element mass matrix $\mathbf{M}_{w,e}$ becomes

$$\mathbf{M}_{w,e} = \rho_w \Delta x_0 \omega_q \mathbf{N}_{eq}^T \mathbf{N}_{eq}, \tag{4.35}$$

with Gaussian weight $\omega_q = 1$, following the integral bounds. This is equivalent to

$$\mathbf{M}_{w,e} = \frac{\rho_w \Delta x_0}{4} \begin{bmatrix} 1 & 1 \\ 1 & 1 \end{bmatrix}. \tag{4.36}$$

Finally, the global mass matrix $\mathbf{M}_w$ is assembled from the element mass matrices $\mathbf{M}_{w,e}$ according to the assemblage procedure that is explained in Appendix D

$$\mathbf{M}_w = \sum_{e=1}^{n_e} \mathbf{A}_e^T \mathbf{M}_{w,e} \mathbf{A}_e. \tag{4.37}$$

Here, $\mathbf{A}_e$ denote the boolean matrix associated with element e.

Following the MPM code developed by Deltares and partners, the mass matrices $\mathbf{M}_w$, $\mathbf{M}_s$ and $\bar{\mathbf{M}}_w$ and damping matrix $\mathbf{Q}$ are used in lumped form; i.e. in diagonal form. Each diagonal entry of the lumped matrix equals the row sum of the corresponding original matrix, see Appendix E. The lumped mass matrix $\mathbf{M}_w^L$ is for example obtained by assembling the lumped element mass matrices $\mathbf{M}_{w,e}^L$

$$\mathbf{M}_{w,e}^L = \frac{\rho_w \Delta x_0}{2} \begin{bmatrix} 1 & 0 \\ 0 & 1 \end{bmatrix}. \tag{4.38}$$

It should be noted that the superscript $(\cdot)^L$ is omitted throughout the rest of this thesis, such that $\mathbf{M}_w$ denotes the lumped mass matrix.

The discrete form of the storage equation in Equation 3.13 and constitutive relation in Equation 3.17 are generally presented for the Gauss point inside element e

$$\frac{dp_e}{dt} = \frac{K_w}{n}\left[(1-n)\mathbf{B}_{eq}\mathbf{v}_{s,e} + n\mathbf{B}_{eq}\mathbf{v}_{w,e}\right], \tag{4.39}$$

$$\frac{d\sigma'_e}{dt} = E^c\mathbf{B}_{eq}\mathbf{v}_{s,e}, \tag{4.40}$$

with nodal velocities

$$\mathbf{v}_{s,e} = \begin{bmatrix} v_{s,i} \\ \\ v_{s,i+1} \end{bmatrix}, \qquad \mathbf{v}_{w,e} = \begin{bmatrix} v_{w,i} \\ \\ v_{w,i+1} \end{bmatrix}. \tag{4.41}$$

However, for the stability analysis in Chapter 5 it is necessary to provide the global equations. Therefore, Equation 4.39 and 4.40 are multiplied with the element step function vector $\mathbf{K}_{eq}$. The resulting element matrices and vectors are subsequently assembled to global matrices and vectors, yielding

$$\frac{d\mathbf{p}}{dt} = \mathbf{K}^s\mathbf{v}_s + \mathbf{K}^w\mathbf{v}_w, \tag{4.42}$$

$$\frac{d\boldsymbol{\sigma}'}{dt} = \bar{\mathbf{K}}^s\mathbf{v}_s, \tag{4.43}$$

with element matrices

$$\mathbf{K}^s_e = \frac{1-n}{n}K_w\mathbf{K}^T_{eq}\mathbf{B}_{eq}, \tag{4.44}$$

$$\mathbf{K}^w_e = K_w\mathbf{K}^T_{eq}\mathbf{B}_{eq}, \tag{4.45}$$

$$\bar{\mathbf{K}}^s_e = E^c\mathbf{K}^T_{eq}\mathbf{B}_{eq}. \tag{4.46}$$

4.2. EULER-CROMER METHOD

In the previous section the partial differential equations were spatially discretized resulting in a system of coupled ordinary differential equations. In this section the Euler-Cromer method is applied to this system of ordinary differential equations for discretization with respect to time. The Euler-Cromer method is a semi-implicit time-stepping scheme in which the velocities are updated explicitly and the effective stress and pore pressure implicitly.

The Euler-Cromer method has been chosen after elimination of other schemes. Implicit schemes were not considered because of the need for matrix inversion processes, which are time-consuming. On the other hand, the explicit Euler forward scheme is unstable; i.e. it renders an unphysical increase in energy with every time step [22]. Cromer [18] showed that with a slight modification a conservative scheme could be obtained, now known as the Euler-Cromer method. The only disadvantage of the Euler-Cromer method is the fact that it is conditionally stable, meaning that the time step size is restricted.

Recall the system of ordinary differential equations, as obtained in Section 4.1

$$\mathbf{M}_w \frac{d\mathbf{v}_w}{dt} = \mathbf{F}^{trac,w} - \mathbf{K}^p \mathbf{p} + \mathbf{F}^{grav,w} - \mathbf{Q}(\mathbf{v}_w - \mathbf{v}_s), \tag{4.47}$$

$$\mathbf{M}_s \frac{d\mathbf{v}_s}{dt} = -\bar{\mathbf{M}}_w \frac{d\mathbf{v}_w}{dt} + \mathbf{F}^{trac} - \mathbf{K}^\sigma(\boldsymbol{\sigma}' + \mathbf{p}) + \mathbf{F}^{grav}, \tag{4.48}$$

$$\frac{d\mathbf{p}}{dt} = \mathbf{K}^s \mathbf{v}_s + \mathbf{K}^w \mathbf{v}_w, \tag{4.49}$$

$$\frac{d\boldsymbol{\sigma}'}{dt} = \bar{\mathbf{K}}^s \mathbf{v}_s. \tag{4.50}$$

The application of the Euler-Cromer method to the 2-phase formulation requires Equation 4.47 and 4.48 to be solved explicitly

$$\mathbf{v}_w^{n+1} = \mathbf{v}_w^n + \Delta t \mathbf{M}_w^{-1} \left[\mathbf{F}^{trac,w} - \mathbf{K}^p \mathbf{p}^n + \mathbf{F}^{grav,w} - \mathbf{Q}(\mathbf{v}_w^n - \mathbf{v}_s^n) \right], \tag{4.51}$$

$$\mathbf{v}_s^{n+1} = \mathbf{v}_s^n + \Delta t \mathbf{M}_s^{-1} \left[-\bar{\mathbf{M}}_w \left(\frac{\mathbf{v}_w^{n+1} - \mathbf{v}_w^n}{\Delta t} \right) + \mathbf{F}^{trac} - \mathbf{K}^\sigma(\boldsymbol{\sigma}'^n + \mathbf{p}^n) + \mathbf{F}^{grav} \right]. \tag{4.52}$$

Equation 4.49 and 4.50, on the other hand, are subsequently solved implicitly

$$\mathbf{p}^{n+1} = \mathbf{p}^n + \Delta t \left[\mathbf{K}^s \mathbf{v}_s^{n+1} + \mathbf{K}^w \mathbf{v}_w^{n+1} \right], \tag{4.53}$$

$$\boldsymbol{\sigma}'^{n+1} = \boldsymbol{\sigma}'^n + \Delta t \left[\bar{\mathbf{K}}^s \mathbf{v}_s^{n+1} \right]. \tag{4.54}$$

It should be noted that no matrix inversion processes are required to solve Equation 4.53 and 4.54, since the updated velocities are already calculated in Equation 4.51 and 4.52.

The starting point of this algorithm is the set of discrete initial conditions

$$\mathbf{v}_s^0 = \begin{bmatrix} \hat{v}_{s,0}(x_1) \\ \vdots \\ \hat{v}_{s,0}(x_{n_n}) \end{bmatrix}, \quad \mathbf{v}_w^0 = \begin{bmatrix} \hat{v}_{w,0}(x_1) \\ \vdots \\ \hat{v}_{w,0}(x_{n_n}) \end{bmatrix}, \quad \mathbf{p}^0 = \begin{bmatrix} \hat{p}_0(x_1) \\ \vdots \\ \hat{p}_0(x_{n_e}) \end{bmatrix}, \quad \boldsymbol{\sigma}'^0 = \begin{bmatrix} \hat{\sigma}'_0(x_1) \\ \vdots \\ \hat{\sigma}'_0(x_{n_e}) \end{bmatrix}. \tag{4.55}$$

4.3. VALIDATION

In this section two dynamic geotechnical problems are solved using the 2-phase formulation as presented in Section 4.1 and 4.2. The problem of one-dimensional wave propagation is first addressed, followed by the problem of one-dimensional consolidation. Both problems, inspired by the benchmarks in [22], are presented for validation of a Matlab implementation that is used during the study of numerical stability in the following chapter. Numerical results are therefore compared to the corresponding analytical solutions.

ONE-DIMENSIONAL WAVE PROPAGATION

In this benchmark a 2 m high column of saturated soil is considered with zero displacement and zero flux conditions at the bottom. Initially the material is at rest. Gravity is neglected. A compressive total stress and pressure of 10 kPa are instantaneously applied and maintained at the top of the column at the beginning of the simulation, implying undrained conditions. The exemplary material properties listed in Table 4.1 are considered in this benchmark.

ρ_s	=	2600	kg/m^3	ρ_w	=	1000	kg/m^3
E^c	=	2500	MPa	K_w	=	2000	MPa
n	=	0.4					

Table 4.1: List of exemplary material properties

The applied load is initially distributed over the pore water and the soil skeleton, proportional to the respective stiffness K_w/n and E^c. The pore pressure will increase by

$$\Delta p = \frac{K_w/n}{E^c + K_w/n}\bar{\sigma} = \frac{2}{3}\bar{\sigma}, \tag{4.56}$$

while the effective stress will increase by

$$\Delta\sigma' = \frac{E^c}{E^c + K_w/n}\bar{\sigma} = \frac{1}{3}\bar{\sigma}. \tag{4.57}$$

According to Verruijt [24], two waves can be observed upon sudden loading. The first wave is an undrained wave that is characterized by soil and water moving with the same velocity. The wave speed is given by

$$c_1 = \sqrt{\frac{E^c + K_w/n}{\rho_{sat}}} = 1956\ m/s. \tag{4.58}$$

The second wave is characterized by soil and water moving in opposite directions. This wave is called the damped wave. It is generally slower than the undrained wave

$$c_2 = \sqrt{\frac{nE^c}{(1-n)K_w + nE^c}}\sqrt{\frac{K_w}{\rho_w}} = 953\ m/s. \tag{4.59}$$

To capture the wave propagation properly, a fine mesh of 800 line elements is considered, each having initial length $\Delta x_0 = 0.0025\ m$. The time step size is set to 0.000001 s, which means that 3000 time steps are necessary to span a time interval of 0.003 s.

At first, a low permeability of $k = 10^{-5}\ m/s$ is considered. Since the damped wave can only be observed in the vicinity of the loading source, only the undrained wave is visible at a depth of 0.5 m, see Figure 4.4 and 4.5. The numerical solution fully coincides with the analytical solution of the problem so that only one line is visible. It should be noted that the analytical solution is obtained for a semi-infinite column [24] taking into account reflection at the bottom of the column.

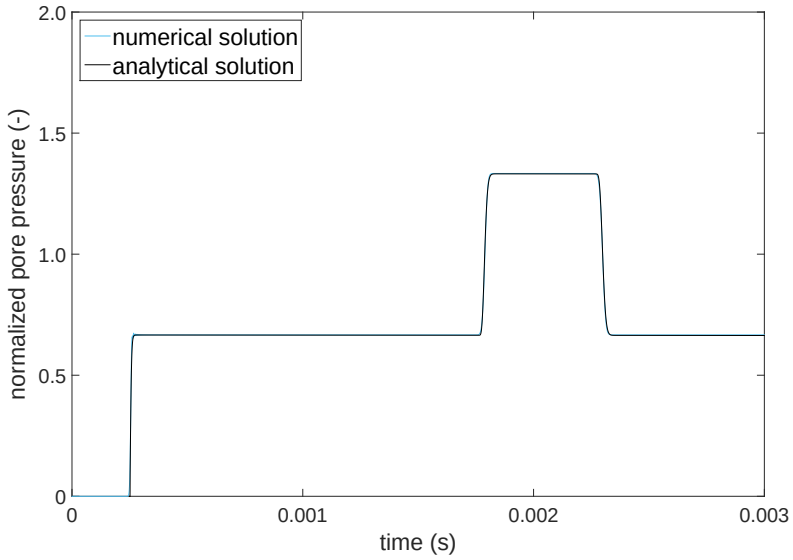

Figure 4.4: Normalized pore pressure $\hat{p}/\bar{\sigma}$ at $x_0 = 1.5\ m$ for the case of a low permeability of $k = 10^{-5}\ m/s$

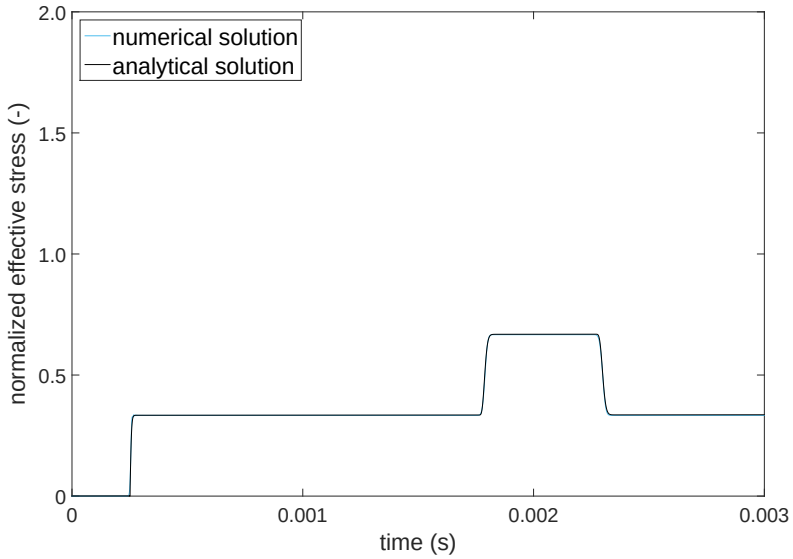

Figure 4.5: Normalized effective stress $\hat{\sigma}'/\bar{\sigma}$ at $x_0 = 1.5\ m$ for the case of a low permeability of $k = 10^{-5}\ m/s$

Results for a high permeability of $k = 10^{-3}\ m/s$ are shown in Figure 4.6 and 4.7. Oscillations are noticed in the numerical solution, but it globally matches with the analytical solution. The oscillations can be explained by a low damping through the term of Equation 4.25.

Another consequence of the low damping is the damped wave reaching deep enough to be visible at a depth of 0.5 m. It should be noted that the effect of the damped wave on the effective stress is opposite to the pore pressure.

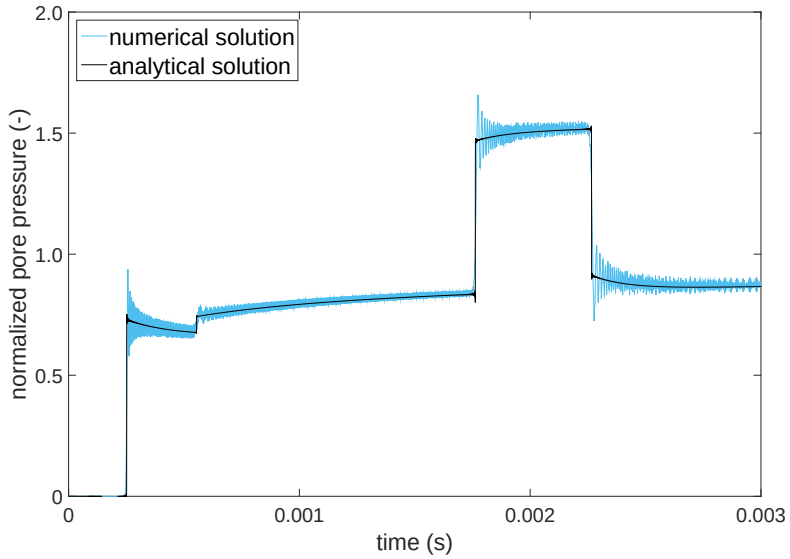

Figure 4.6: Normalized pore pressure $\hat{p}/\bar{\sigma}$ at $x_0 = 1.5\ m$ for the case of a high permeability of $k = 10^{-3}\ m/s$

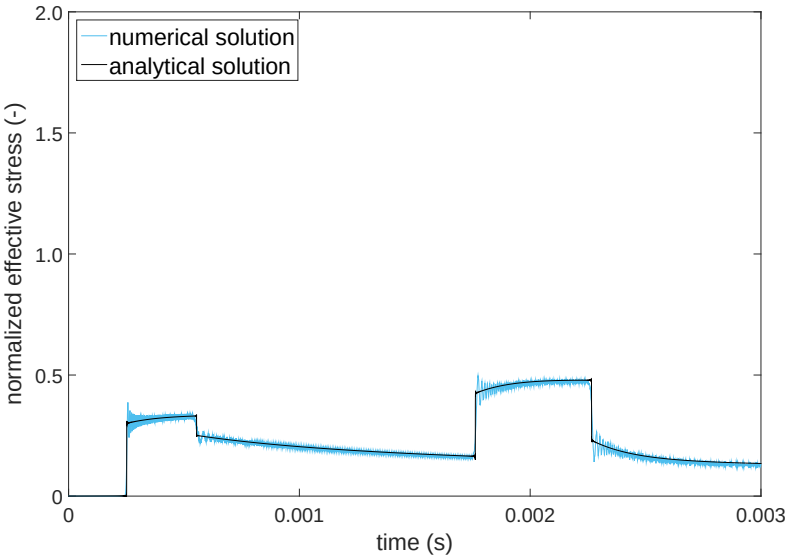

Figure 4.7: Normalized effective stress $\hat{\sigma}'/\bar{\sigma}$ at $x_0 = 1.5\ m$ for the case of a high permeability of $k = 10^{-3}\ m/s$

ONE-DIMENSIONAL CONSOLIDATION

In the second benchmark test a 1.0 m high column of saturated soil is considered with the material properties listed in Table 4.2. Zero displacement and zero flux conditions are assumed at the bottom and a compressive load of 10 kPa is applied at the top surface of the soil, slowly squeezing the water out of the pores. The material has again zero initial conditions for the displacement and velocities. The load is assumed to be initially fully carried by the water phase. This implies initial conditions

$$\hat{p}_0 = -10\ kPa \qquad \text{and} \qquad \hat{\sigma}'_0 = 0\ kPa. \tag{4.60}$$

For these calculations the column is divided into 100 elements of size $\Delta x_0 = 0.01\ m$. The time step size is again set to 0.000001 s.

ρ_s	=	2600 kg/m^3	ρ_w	=	1000 kg/m^3
E^c	=	2500 MPa	K_w	=	2000 MPa
n	=	0.4			

Table 4.2: List of exemplary material properties

The dissipation of the excess pore pressure is captured by the one-dimensional consolidation equation [10]

$$\frac{\partial \hat{p}}{\partial t} = c_v \frac{\partial^2 \hat{p}}{\partial x_0^2}, \tag{4.61}$$

with consolidation coefficient

$$c_v = \frac{k}{\rho_w g (1/E^c + n/K_w)}. \tag{4.62}$$

The coefficient is a measure for the rate of consolidation. It deviates from the common notation, because of the assumed compressibility of the water [24].

Figure 4.8 presents the dissipation of excess pore pressure for the case of a low permeability of $k = 10^{-5}\ m/s$. The results are shown for various values of dimensionless time T, given by

$$T = \frac{c_v t}{H^2}. \tag{4.63}$$

Owing to the low permeability and consequently low consolidation coefficient, the consolidation process is slow and the undrained wave is almost damped out before the first result is plotted for $T = 0.02$. The numerical solution therefore matches with the analytical solution of Equation 4.61 which does not take into account the undrained wave.

Figure 4.9 corresponds to the case of a high permeability of $k = 10^{-3}\ m/s$. The consolidation process is much faster. The undrained wave and its reflections are still apparent and the numerical solution only roughly matches with the analytical solution for $T \geq 0.2$. The numerical solution slowly converges to the analytical solution due to the undrained wave damping out.

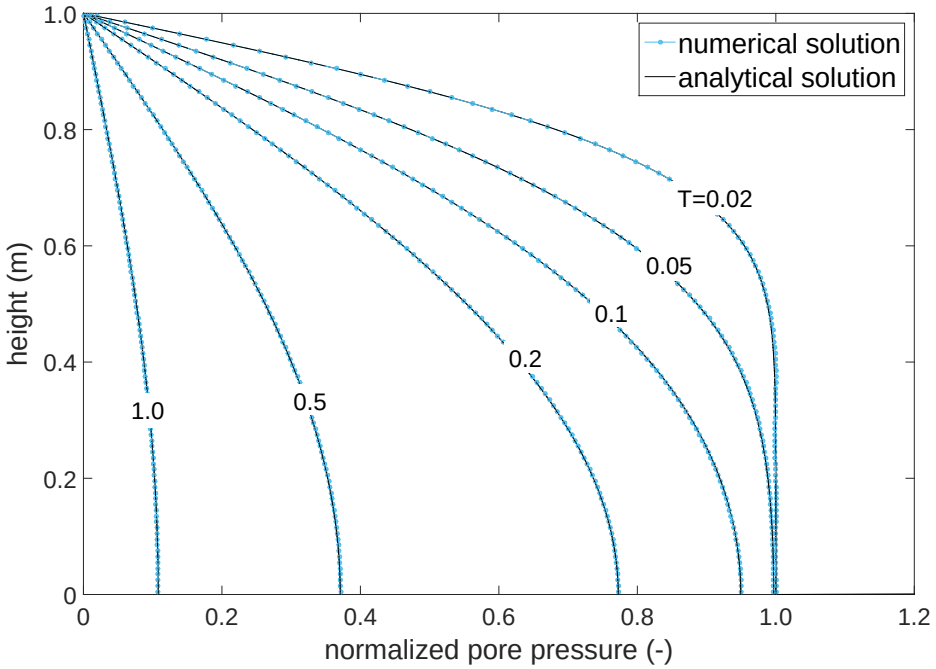

Figure 4.8: Normalized pore pressure profile ($\hat{p}/\hat{p}_0$) at various dimensionless times T for the case of a low permeability of $k = 10^{-5}\ m/s$

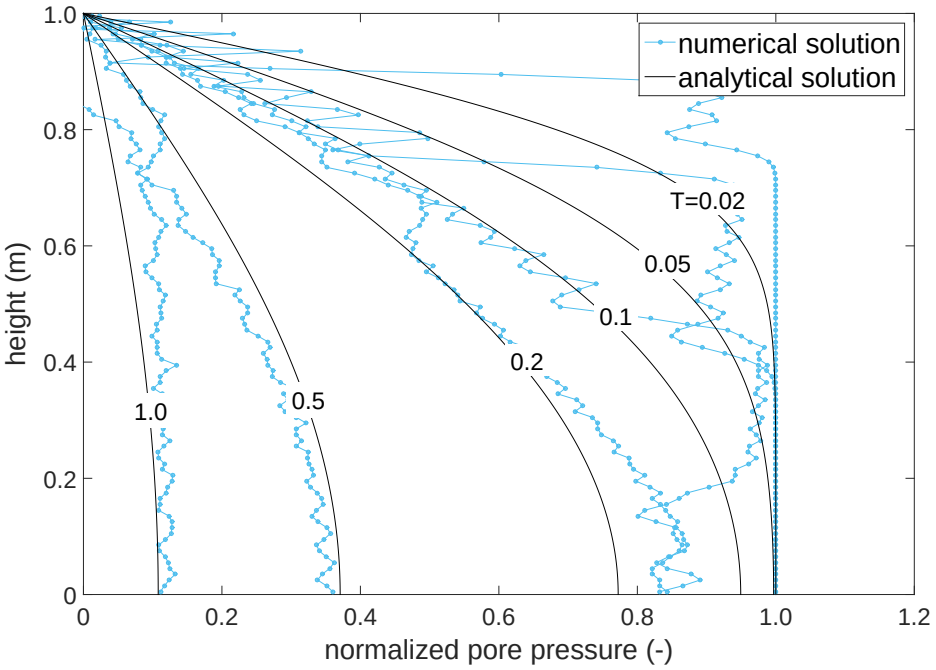

Figure 4.9: Normalized pore pressure profile ($\hat{p}/\hat{p}_0$) at various dimensionless times T for the case of a high permeability of $k = 10^{-3}\ m/s$

5

STABILITY ANALYSIS

Chapter 4 presented and validated the finite element space discretization and Euler-Cromer time discretization of the velocity-based 2-phase formulation. Since the Euler-Cromer scheme is conditionally stable, the time step size has to satisfy a stability criterion for a performed analysis to be stable. The Courant-Friedrich-Lewy condition [8] for undrained wave propagation was found to be insufficient. A permeability-dependent criterion was then identified by studying one-dimensional consolidation with the assumption of an incompressible pore fluid [9]. However, this new criterion, though providing a useful guideline for estimating the critical time step size, proved to be insufficient, too.

This chapter presents the stability analysis of the velocity-based 2-phase formulation without the extra assumption used in [9] in order to obtain a sufficient criterion. In Section 5.1, the matrix method is applied to the system of ordinary differential equations obtained after the finite element space discretization. Then, in Section 5.2, the matrix method is applied to the system of discrete equations obtained after introducing the Euler-Cromer time discretization. Both analyses render an estimate of the critical time step size. However, the combination of both provides a more accurate result. This heuristic result is presented in Section 5.3. Finally, all obtained estimates are validated and compared in Section 5.4.

5.1. MATRIX METHOD APPLIED TO ORDINARY DIFFERENTIAL EQUATIONS

Hirsch [25] describes the matrix method as a stability analysis method that reduces the system of ordinary differential equations to scalar test functions by performing an eigenvalue decomposition. The Euler-Cromer time discretization is subsequently applied to these test functions. The resulting discrete equations can be analyzed to obtain a stability criterion.

The system of ordinary differential equations obtained in Section 4.1 is repeated here

$$\mathbf{M}_w \frac{d\mathbf{v}_w}{dt} = \mathbf{F}^{trac,w} - \mathbf{K}^p \mathbf{p} + \mathbf{F}^{grav,w} - \mathbf{Q}(\mathbf{v}_w - \mathbf{v}_s), \tag{5.1}$$

$$\mathbf{M}_s \frac{d\mathbf{v}_s}{dt} = -\bar{\mathbf{M}}_w \frac{d\mathbf{v}_w}{dt} + \mathbf{F}^{trac} - \mathbf{K}^\sigma(\boldsymbol{\sigma}' + \mathbf{p}) + \mathbf{F}^{grav}, \tag{5.2}$$

$$\frac{d\mathbf{p}}{dt} = \mathbf{K}^s \mathbf{v}_s + \mathbf{K}^w \mathbf{v}_w, \tag{5.3}$$

$$\frac{d\boldsymbol{\sigma}'}{dt} = \bar{\mathbf{K}}^s \mathbf{v}_s. \tag{5.4}$$

Considering that $\mathbf{v}_s = \frac{d\mathbf{u}_s}{dt}$ and $\mathbf{v}_w = \frac{d\mathbf{u}_w}{dt}$, we are able to reduce the number of equations to

$$\mathbf{M}_w \frac{d^2\mathbf{u}_w}{dt^2} = \mathbf{F}^{trac,w} - \mathbf{K}^p(\mathbf{K}^s\mathbf{u}_s + \mathbf{K}^w\mathbf{u}_w) + \mathbf{F}^{grav,w} - \mathbf{Q}\left(\frac{d\mathbf{u}_w}{dt} - \frac{d\mathbf{u}_s}{dt}\right), \tag{5.5}$$

$$\mathbf{M}_s \frac{d^2\mathbf{u}_s}{dt^2} = -\bar{\mathbf{M}}_w \frac{d^2\mathbf{u}_w}{dt^2} + \mathbf{F}^{trac} - \mathbf{K}^\sigma(\bar{\mathbf{K}}^s\mathbf{u}_s + \mathbf{K}^s\mathbf{u}_s + \mathbf{K}^w\mathbf{u}_w) + \mathbf{F}^{grav}. \tag{5.6}$$

In matrix notation this becomes

$$\begin{bmatrix} \mathbf{0} & \mathbf{M}_w \\ \mathbf{M}_s & \bar{\mathbf{M}}_w \end{bmatrix} \begin{bmatrix} \frac{d^2\mathbf{u}_s}{dt^2} \\ \frac{d^2\mathbf{u}_w}{dt^2} \end{bmatrix} + \begin{bmatrix} -\mathbf{Q} & \mathbf{Q} \\ \mathbf{0} & \mathbf{0} \end{bmatrix} \begin{bmatrix} \frac{d\mathbf{u}_s}{dt} \\ \frac{d\mathbf{u}_w}{dt} \end{bmatrix} + \begin{bmatrix} \mathbf{K}^p\mathbf{K}^s & \mathbf{K}^p\mathbf{K}^w \\ \mathbf{K}^\sigma\bar{\mathbf{K}}^s + \mathbf{K}^\sigma\mathbf{K}^s & \mathbf{K}^\sigma\mathbf{K}^w \end{bmatrix} \begin{bmatrix} \mathbf{u}_s \\ \mathbf{u}_w \end{bmatrix} = \begin{bmatrix} \mathbf{F}^1 \\ \mathbf{F}^2 \end{bmatrix}. \tag{5.7}$$

We will refer to the matrices as the mass matrix, damping matrix and stiffness matrix, respectively. The vector on the right hand side includes all non-homogeneous terms. It can be neglected in stability analyses.

Since the damping matrix is not a linear combination of the mass matrix and the stiffness matrix as in [9], it is necessary to solve the quadratic eigenvalue problem

$$\begin{bmatrix} \mathbf{0} & \mathbf{M}_w \\ \mathbf{M}_s & \bar{\mathbf{M}}_w \end{bmatrix} \lambda^2 - \begin{bmatrix} -\mathbf{Q} & \mathbf{Q} \\ \mathbf{0} & \mathbf{0} \end{bmatrix} \lambda + \begin{bmatrix} \mathbf{K}^p\mathbf{K}^s & \mathbf{K}^p\mathbf{K}^w \\ \mathbf{K}^\sigma\bar{\mathbf{K}}^s + \mathbf{K}^\sigma\mathbf{K}^s & \mathbf{K}^\sigma\mathbf{K}^w \end{bmatrix} = 0, \tag{5.8}$$

which is obtained by substituting $\mathbf{C}_s e^{-\lambda t}$ and $\mathbf{C}_w e^{-\lambda t}$ for the variables $\mathbf{u}_s$ and $\mathbf{u}_w$, respectively.

Irons [26] proved that each eigenvalue λ is a weighted mean of the element eigenvalues λ_e. Therefore, the element matrices can be substituted for the global matrices in Equation 5.8 in order to calculate the element eigenvalues λ_e. The characteristic equation corresponding to the elemental equivalent of Equation 5.8 is

$$\frac{1}{16}(1-n)^2\rho_s^2\rho_w^2\Delta x_0^4\lambda_e^3(\lambda_e - a)\left(\lambda_e^4 - a\lambda_e^3 + b\lambda_e^2 - c\lambda_e + d\right) = 0, \tag{5.9}$$

with positive coefficients

$$a = \frac{n\rho_{sat}g}{(1-n)\rho_s k}, \tag{5.10}$$

$$b = \frac{4\left(n\rho_{sat}K_w + (1-2n)\rho_w K_w + n\rho_w E^c\right)}{n(1-n)\rho_s\rho_w\Delta x_0^2}, \tag{5.11}$$

$$c = \frac{4g\,(nE^c + K_w)}{(1-n)\rho_s k\Delta x_0^2}, \tag{5.12}$$

$$d = \frac{16K_w E^c}{(1-n)\rho_s\rho_w\Delta x_0^4}. \tag{5.13}$$

It is easy to determine that the first four roots of Equation 5.9 are

$$\lambda_e = 0, \quad \lambda_e = 0, \quad \lambda_e = 0, \quad \lambda_e = a. \tag{5.14}$$

In order to find the remaining roots, it is necessary to solve the quartic equation that is part of Equation 5.9. This 4th order equation can be solved analytically, see e.g. Shmakov [27]. However, the analytical solution is difficult to work with, since it is a complex combination of square and cube roots. We will therefore only look at limit cases, expecting to obtain a rough estimate for the critical time step size.

First, we search for mesh-dependent eigenvalues by taking the limit $k \to \infty$. In this case $a \to 0$ and $c \to 0$, such that the quartic equation becomes

$$\lambda_e^4 + b\lambda_e^2 + d = 0. \tag{5.15}$$

Equation 5.15 has imaginary roots

$$\lambda_e = \pm i\sqrt{\frac{1}{2}\left(b - \sqrt{b^2 - 4d}\right)}, \qquad \lambda_e = \pm i\sqrt{\frac{1}{2}\left(b + \sqrt{b^2 - 4d}\right)}. \tag{5.16}$$

On the other hand, we take the limit $\Delta x \to \infty$ to obtain permeability-dependent eigenvalues, yielding the quartic equation

$$\lambda_e^4 - a\lambda_e^3 = 0, \tag{5.17}$$

with real roots

$$\lambda_e = 0, \qquad \lambda_e = 0, \qquad \lambda_e = 0, \qquad \lambda_e = a. \tag{5.18}$$

Each of the obtained eigenvalues results in a scalar test function, being

$$\frac{d^2\hat{u}}{dt^2} = -\mathrm{Re}(\lambda)\frac{d\hat{u}}{dt} - \mathrm{Im}(\lambda)^2\hat{u}. \tag{5.19}$$

This test function is representative, since the real part of the eigenvalue is a damping constant and the imaginary part of the eigenvalue is a frequency.

When the Euler-Cromer scheme is applied to the test function in Equation 5.19, we find the discrete system

$$v^{n+1} = v^n - \mathrm{Re}(\lambda)\Delta t v^n - \mathrm{Im}(\lambda)^2\Delta t u^n, \tag{5.20}$$

$$u^{n+1} = u^n + \Delta t v^{n+1}. \tag{5.21}$$

In matrix notation this becomes

$$\begin{bmatrix} v^{n+1} \\ u^{n+1} \end{bmatrix} = \begin{bmatrix} 1 - \mathrm{Re}(\lambda)\Delta t & -\mathrm{Im}(\lambda)^2\Delta t \\ \Delta t - \mathrm{Re}(\lambda)\Delta t^2 & 1 - \mathrm{Im}(\lambda)^2\Delta t^2 \end{bmatrix} \begin{bmatrix} v^n \\ u^n \end{bmatrix}. \tag{5.22}$$

The eigenvalues μ belonging to the amplification matrix in Equation 5.22 are

$$\mu = 1 - \frac{1}{2}\mathrm{Re}(\lambda)\Delta t - \frac{1}{2}\mathrm{Im}(\lambda)^2\Delta t^2 \pm \sqrt{\left(1 - \frac{1}{2}\mathrm{Re}(\lambda)\Delta t - \frac{1}{2}\mathrm{Im}(\lambda)^2\Delta t^2\right)^2 - (1 - \mathrm{Re}(\lambda)\Delta t)}. \tag{5.23}$$

Lemma 5.1. *Let a, b be real numbers that satisfy the inequality*

$$\left| a \pm \sqrt{a^2 - b} \right| \leq 1.$$

Then a, b satisfy

$$-b - 1 \leq 2a \leq b + 1 \quad \text{and} \quad b \leq 1.$$

By definition, the numerical method is stable when $|\mu| \leq 1$. This expression can be simplified with Lemma 5.1, presented and proven in [9], yielding

$$-2 + \mathrm{Re}(\lambda)\Delta t \leq 2 - \mathrm{Re}(\lambda)\Delta t - \mathrm{Im}(\lambda)^2\Delta t^2 \leq 2 - \mathrm{Re}(\lambda)\Delta t \quad \text{and} \quad 1 - \mathrm{Re}(\lambda)\Delta t \leq 1. \tag{5.24}$$

This is equivalent to

$$\mathrm{Im}(\lambda)^2\Delta t^2 + 2\mathrm{Re}(\lambda)\Delta t - 4 \leq 0, \quad \mathrm{Im}(\lambda)^2\Delta t^2 \geq 0 \quad \text{and} \quad \mathrm{Re}(\lambda)\Delta t \geq 0. \tag{5.25}$$

It should be noted that the zero element eigenvalues always satisfy the criteria in Equation 5.25, while the nonzero element eigenvalues only satisfy the criteria under specific conditions. For real eigenvalues these conditions can be written as

$$0 \leq \Delta t \leq \frac{2}{\mathrm{Re}(\lambda)}. \tag{5.26}$$

For complex eigenvalues the time step size must satisfy

$$0 \leq \Delta t \leq \frac{-\mathrm{Re}(\lambda) + \sqrt{\mathrm{Re}(\lambda)^2 + 4\mathrm{Im}(\lambda)^2}}{\mathrm{Im}(\lambda)^2}, \tag{5.27}$$

which reduces to

$$0 \leq \Delta t \leq \frac{2}{|\mathrm{Im}(\lambda)|} \tag{5.28}$$

when the real part is zero.

From the stability criteria that are obtained from all nonzero element eigenvalues in the limit cases, we find an estimate for the critical time step size. It is given by

$$\Delta t_{crit,1} = \min\left(\frac{2}{a}, \frac{2\sqrt{2}}{\sqrt{b + \sqrt{b^2 - 4d}}} \right). \tag{5.29}$$

5.2. MATRIX METHOD APPLIED TO DISCRETE EQUATIONS

Hoffman [28] does not perform the eigenvalue decomposition to the system of ordinary differential equations, but to the system of discrete equations. This system is obtained in Section 4.2 and repeated here

$$\mathbf{v}_w^{n+1} = \mathbf{v}_w^n + \Delta t \mathbf{M}_w^{-1}\left[\mathbf{F}^{trac,w} - \mathbf{K}^p\mathbf{p}^n + \mathbf{F}^{grav,w} - \mathbf{Q}(\mathbf{v}_w^n - \mathbf{v}_s^n)\right], \tag{5.30}$$

$$\mathbf{v}_s^{n+1} = \mathbf{v}_s^n + \Delta t \mathbf{M}_s^{-1}\left[-\bar{\mathbf{M}}_w\left(\frac{\mathbf{v}_w^{n+1}-\mathbf{v}_w^n}{\Delta t}\right) + \mathbf{F}^{trac} - \mathbf{K}^\sigma(\boldsymbol{\sigma}'^n + \mathbf{p}^n) + \mathbf{F}^{grav}\right], \tag{5.31}$$

$$\mathbf{p}^{n+1} = \mathbf{p}^n + \Delta t\left[\mathbf{K}^s\mathbf{v}_s^{n+1} + \mathbf{K}^w\mathbf{v}_w^{n+1}\right], \tag{5.32}$$

$$\boldsymbol{\sigma}'^{n+1} = \boldsymbol{\sigma}'^n + \Delta t\left[\bar{\mathbf{K}}^s\mathbf{v}_s^{n+1}\right]. \tag{5.33}$$

However, it is preferable to work with the discrete variant of Equation 5.5 and 5.6, given by

$$\mathbf{v}_w^{n+1} = \mathbf{v}_w^n + \Delta t\mathbf{M}_w^{-1}\left[\mathbf{F}^{trac,w} - \mathbf{K}^p\left(\mathbf{K}^s\mathbf{u}_s^n + \mathbf{K}^w\mathbf{u}_w^n\right) + \mathbf{F}^{grav,w} - \mathbf{Q}\left(\mathbf{v}_w^n - \mathbf{v}_s^n\right)\right], \tag{5.34}$$

$$\mathbf{v}_s^{n+1} = \mathbf{v}_s^n + \Delta t\mathbf{M}_s^{-1}\left[-\bar{\mathbf{M}}_w\left(\frac{\mathbf{v}_w^{n+1}-\mathbf{v}_w^n}{\Delta t}\right) + \mathbf{F}^{trac} - \mathbf{K}^\sigma\left(\bar{\mathbf{K}}^s\mathbf{u}_s^n + \mathbf{K}^s\mathbf{u}_s^n + \mathbf{K}^w\mathbf{u}_w^n\right) + \mathbf{F}^{grav}\right], \tag{5.35}$$

$$\mathbf{u}_w^{n+1} = \mathbf{u}_w^n + \Delta t\mathbf{v}_w^{n+1}, \tag{5.36}$$

$$\mathbf{u}_s^{n+1} = \mathbf{u}_s^n + \Delta t\mathbf{v}_s^{n+1}. \tag{5.37}$$

The amplification matrix belonging to this system of discrete equations equals

$$\mathbf{G} = \begin{bmatrix} \mathbf{I} - \Delta t\mathbf{M}_w^{-1}\mathbf{Q} & \Delta t\mathbf{M}_w^{-1}\mathbf{Q} & -\Delta t\mathbf{M}_w^{-1}\mathbf{K}^p\mathbf{K}^w & -\Delta t\mathbf{M}_w^{-1}\mathbf{K}^p\mathbf{K}^s \\ n\,\Delta t\mathbf{M}_s^{-1}\mathbf{Q} & \mathbf{I} - n\Delta t\mathbf{M}_s^{-1}\mathbf{Q} & -(1-n)\Delta t\mathbf{M}_s^{-1}\mathbf{K}^p\mathbf{K}^w & \begin{matrix}-\Delta t\mathbf{M}_s^{-1}\mathbf{K}^\sigma\bar{\mathbf{K}}^s \\ -(1-n)\Delta t\mathbf{M}_s^{-1}\mathbf{K}^p\mathbf{K}^s\end{matrix} \\ \Delta t\mathbf{I} - \Delta t^2\mathbf{M}_w^{-1}\mathbf{Q} & \Delta t^2\mathbf{M}_w^{-1}\mathbf{Q} & \mathbf{I} - \Delta t^2\mathbf{M}_w^{-1}\mathbf{K}^p\mathbf{K}^w & -\Delta t^2\mathbf{M}_w^{-1}\mathbf{K}^p\mathbf{K}^s \\ n\,\Delta t^2\mathbf{M}_s^{-1}\mathbf{Q} & \Delta t\mathbf{I} - n\Delta t^2\mathbf{M}_s^{-1}\mathbf{Q} & -(1-n)\Delta t^2\mathbf{M}_s^{-1}\mathbf{K}^p\mathbf{K}^w & \begin{matrix}\mathbf{I} - \Delta t^2\mathbf{M}_s^{-1}\mathbf{K}^\sigma\bar{\mathbf{K}}^s \\ -(1-n)\Delta t^2\mathbf{M}_s^{-1}\mathbf{K}^p\mathbf{K}^s\end{matrix} \end{bmatrix}. \tag{5.38}$$

As in the previous section, application of Irons' theorem [26] reduces the complexity of the eigenvalue decomposition of the amplification matrix $\mathbf{G}$. In this case, the eigenvalues μ_e of the element amplification matrices $\mathbf{G}_e$ are calculated, which are constructed by replacing the global matrices in Equation 5.38 by the corresponding element matrices. The characteristic equation that belongs to this eigenvalue decomposition becomes

$$\begin{aligned}&(\mu_e - 1)^3(\mu_e - (1-a\Delta t))\left(\mu_e^4 + (-4 + a\Delta t + b\Delta t^2)\mu_e^3\right. \\ &\left. + (6 - 3a\Delta t - 2b\Delta t^2 + c\Delta t^3 + d\Delta t^4)\mu_e^2 + (-4 + 3a\Delta t + b\Delta t^2 - c\Delta t^3)\mu_e + (1 - a\Delta t)\right) = 0.\end{aligned} \tag{5.39}$$

with the coefficients a, b, c and d as defined in Equation 5.10, 5.11, 5.12 and 5.13.

The first four eigenvalues can be explicitly calculated from Equation 5.39

$$\mu_e = 1, \qquad \mu_e = 1, \qquad \mu_e = 1, \qquad \mu_e = 1 - a\Delta t. \tag{5.40}$$

The other four eigenvalues are given by the roots of the remaining quartic equation. The analytical solution again contains square and cube roots, which makes it difficult to deal with.

Instead, Yerro [29] suggests to approximate the eigenvalues by solving the quartic equation

$$\tilde{\mu}_e^4 + \left(-4 + a\Delta t + b\Delta t^2\right)\tilde{\mu}_e^3 + \left(6 - 3a\Delta t - 2b\Delta t^2\right)\tilde{\mu}_e^2 + \left(-4 + 3a\Delta t + b\Delta t^2\right)\tilde{\mu}_e + (1 - a\Delta t) = 0, \tag{5.41}$$

which is obtained by neglecting the terms including Δt^3 and Δt^4 in Equation 5.39, assuming Δt to be small.

The roots of Equation 5.41 give the following approximations for the eigenvalues μ_e

$$\mu_e \approx 1, \qquad \mu_e \approx 1, \qquad \mu_e \approx 1 - \frac{1}{2}a\Delta t - \frac{1}{2}b\Delta t^2 \pm \sqrt{\left(1 - \frac{1}{2}a\Delta t - \frac{1}{2}b\Delta t^2\right)^2 - (1 - a\Delta t)}. \tag{5.42}$$

Using Lemma 5.1, we know that $\left|\mu_e\right| \leq 1$ is satisfied for all approximated eigenvalues μ_e when

$$-2 + a\Delta t \leq 2 - a\Delta t - b\Delta t^2 \leq 2 - a\Delta t, \qquad 1 - a\Delta t \leq 1. \tag{5.43}$$

Since a and b are positive by definition, this is equivalent to

$$0 \leq \Delta t \leq \frac{-a + \sqrt{a^2 + 4b}}{b}. \tag{5.44}$$

The second estimate for the critical time step size is thus given by

$$\Delta t_{crit,2} = \frac{-a + \sqrt{a^2 + 4b}}{b}. \tag{5.45}$$

5.3. HEURISTIC STABILITY CRITERION

In the previous sections two estimates for the critical time step size were obtained. The stability analysis in Section 5.1 resulted in the first estimate, repeated here

$$\Delta t_{crit,1} = \min\left(\frac{2}{a}, \frac{2\sqrt{2}}{\sqrt{b+\sqrt{b^2-4d}}}\right), \tag{5.46}$$

with the coefficients a, b and d as defined in Equation 5.10, 5.11 and 5.13.

In Section 5.2 the second estimate for the critical time step size was obtained, being

$$\Delta t_{crit,2} = \frac{-a+\sqrt{a^2+4b}}{b}. \tag{5.47}$$

Scrutiny of both estimates shows that the expression in Equation 5.46 is a piecewise linear function of the permeability k based on the limit cases $\Delta x_0 \to \infty$ and $k \to \infty$, while the general approximation in Equation 5.47 is a smooth function of the permeability k.

However, it should be noted that the estimates do not coincide for the limit case $k \to \infty$. After all, the latter would imply $a \to 0$, such that

$$\lim_{k\to\infty} \Delta t_{crit,1} = \frac{2\sqrt{2}}{\sqrt{b+\sqrt{b^2-4d}}} \tag{5.48}$$

and

$$\lim_{k\to\infty} \Delta t_{crit,2} = \frac{2}{\sqrt{b}}. \tag{5.49}$$

The difference can be approximated by using Taylor expansions twice, yielding

$$\begin{aligned}
\lim_{k\to\infty} \Delta t_{crit,1} - \lim_{k\to\infty} \Delta t_{crit,2} &= \frac{2\sqrt{2}}{\sqrt{b+\sqrt{b^2-4d}}} - \frac{2}{\sqrt{b}} \\
&\approx \frac{2}{\sqrt{b-\frac{d}{b}}} - \frac{2}{\sqrt{b}} \\
&\approx \frac{2}{\sqrt{b}} + \frac{d}{\sqrt{b^5}} - \frac{2}{\sqrt{b}} \\
&= \frac{d}{\sqrt{b^5}}.
\end{aligned} \tag{5.50}$$

Since Equation 5.48 is exact by definition, a third estimate for the critical time step size is proposed that is obtained by substitution of $\frac{1}{2}\left(b+\sqrt{b^2-4d}\right)$ for b in Equation 5.47, being

$$\Delta t_{crit,3} = \frac{-2a+\sqrt{4a^2+8\left(b+\sqrt{b^2-4d}\right)}}{b+\sqrt{b^2-4d}}. \tag{5.51}$$

This heuristic estimate is a smooth function of the permeability k and satisfies the limit cases.

5.4. VALIDATION

After performing the stability analyses, the three obtained stability criteria must be compared to real critical time step sizes for validation. In order to avoid any ambiguities, the three estimates of the critical time step size are repeated once more. The first and second estimate were obtained in Section 5.1 and 5.2 with two variants of the matrix method, while the third estimate from Section 5.3 is a combination of both

$$\Delta t_{crit,1} = \min\left(\frac{2}{a}, \frac{2\sqrt{2}}{\sqrt{b+\sqrt{b^2-4d}}}\right), \tag{5.52}$$

$$\Delta t_{crit,2} = \frac{-a+\sqrt{a^2+4b}}{b}, \tag{5.53}$$

$$\Delta t_{crit,3} = \frac{-2a+\sqrt{4a^2+8\left(b+\sqrt{b^2-4d}\right)}}{b+\sqrt{b^2-4d}}. \tag{5.54}$$

The coefficients a, b and d in Equations 5.52, 5.53 and 6.16 are given by

$$a = \frac{n\rho_{sat}g}{(1-n)\rho_s k}, \tag{5.55}$$

$$b = \frac{4\left(n\rho_{sat}K_w + (1-2n)\rho_w K_w + n\rho_w E^c\right)}{n(1-n)\rho_s\rho_w\Delta x_0^2}, \tag{5.56}$$

$$d = \frac{16E^c K_w}{(1-n)\rho_s\rho_w\Delta x_0^4}. \tag{5.57}$$

The real values of the critical time step sizes are numerically obtained with calculations on one-dimensional wave propagation, the benchmark presented in Section 4.3. Here, various values of permeability are considered. The critical time step sizes are found by varying the time step size. The results are listed in Table 5.1.

$k\ (m/s)$	$\Delta t_{crit}\ (s)$	$k\ (m/s)$	$\Delta t_{crit}\ (s)$
$1.0\cdot10^{-8}$	$3.98\cdot10^{-9}$	$3.5\cdot10^{-8}$	$1.39\cdot10^{-8}$
$1.0\cdot10^{-7}$	$3.98\cdot10^{-8}$	$3.5\cdot10^{-7}$	$1.39\cdot10^{-7}$
$1.0\cdot10^{-6}$	$3.89\cdot10^{-7}$	$3.5\cdot10^{-6}$	$1.08\cdot10^{-6}$
$1.0\cdot10^{-5}$	$1.24\cdot10^{-6}$	$3.5\cdot10^{-5}$	$1.25\cdot10^{-6}$
$1.0\cdot10^{-4}$	$1.25\cdot10^{-6}$	$3.5\cdot10^{-4}$	$1.25\cdot10^{-6}$
$1.0\cdot10^{-3}$	$1.25\cdot10^{-6}$	$3.5\cdot10^{-3}$	$1.25\cdot10^{-6}$
$1.0\cdot10^{-2}$	$1.25\cdot10^{-6}$		

Table 5.1: Critical time step sizes for various values of permeability obtained from numerical analyses

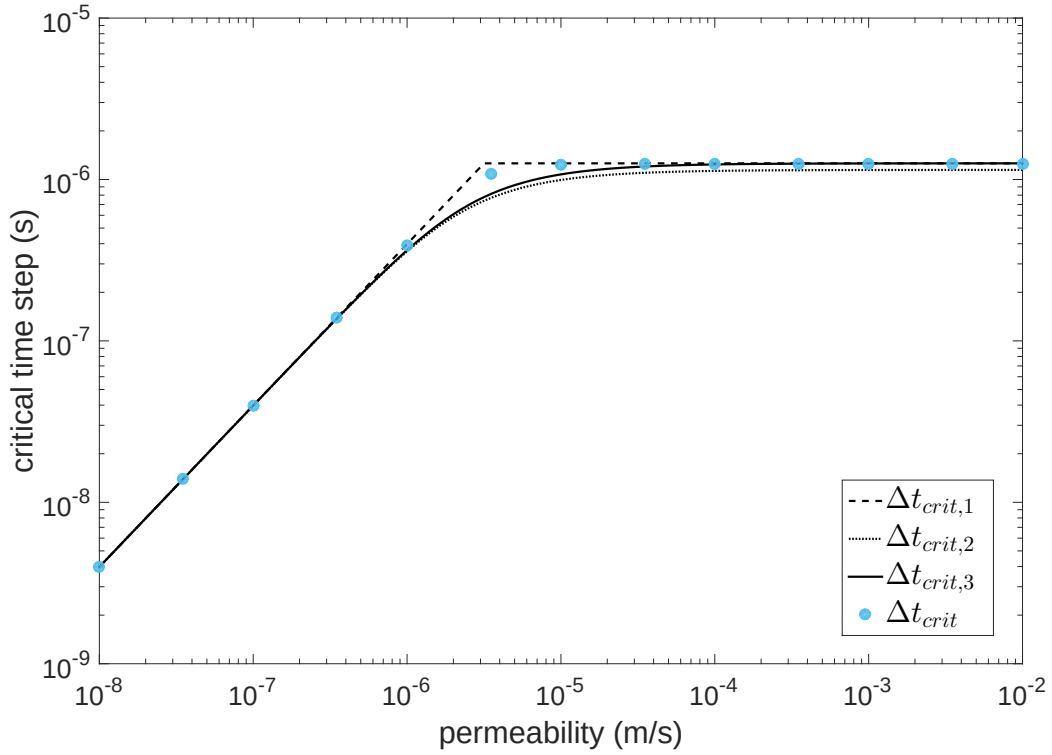

Figure 5.1: Comparison of the obtained stability criteria to the real critical time step sizes

All estimates are plotted in Figure 5.1 as a function of the permeability k, together with the real critical time step sizes Δt_{crit} from Table 5.1 represented by blue dots. We conclude from the figure that the first estimate is not a sufficient criterion, since the dashed line lies above the blue dots. On the other hand, the second and third estimate are sufficient.

A difference is visible between the values in the limit case $k \to \infty$. From the sufficient estimates, the third estimate agrees with the real values, while the second estimate is too low. Following Equation 5.50, the difference is expected to be approximately 10^{-7} s for the parameters considered. This is consistent with the difference of about 10% in Figure 5.1. As a result of this difference, it is the third estimate that is closest to the real critical time step sizes and therefore the recommended one.

In the scope of this study, we compare the third criterion with the two criteria used so far to show the improvement. The Courant-Friedrich-Lewy condition [8] for undrained wave propagation is considered first. This so-called undrained criterion is given by

$$\Delta t_{crit,u} = \frac{\Delta x_0}{\sqrt{(E^c + K_w/n)/\rho_{sat}}}. \tag{5.58}$$

We also consider the permeability-dependent criterion that was obtained during the preliminary study of this thesis [9]. This criterion is based on the analysis of the 2-phase formulation with the assumption of an incompressible pore fluid. Owing to this simplification we refer to it as the simplified criterion $\Delta t_{crit,s}$, being

$$\Delta t_{crit,s} = \min\left(\frac{\Delta x_0}{\sqrt{E^c/\tilde{\rho}}}, \frac{2\tilde{\rho}k}{\rho_w g} \right), \tag{5.59}$$

with

$$\tilde{\rho} = \rho_{sat} + \left(\frac{1}{n} - 2 \right) \rho_w. \tag{5.60}$$

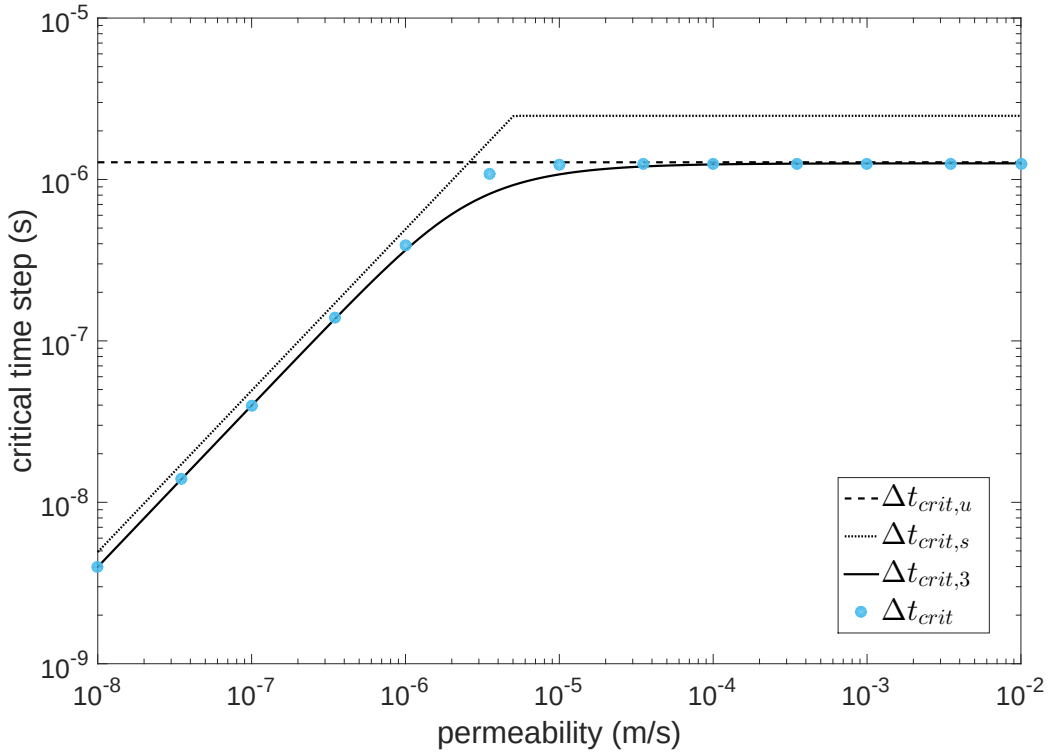

Figure 5.2: Comparison of existing and obtained stability criteria to the real critical time step sizes

Figure 5.2 shows the comparison of the undrained criterion $\Delta t_{crit,u}$, simplified criterion $\Delta t_{crit,s}$ and third criterion $\Delta t_{crit,3}$ for various values of permeability. The real critical time step sizes Δt_{crit} serve as reference values.

Mieremet et al. [30] propose to combine the undrained and simplified criterion, such that the simplified criterion is critical for low permeability and the undrained criterion for high permeability. Figure 5.2 emphasizes this statement and also shows the improvement obtained from switching to the third criterion. This improvement is mostly visible in the range of low permeabilities. However, although hardly visible, improvement is also present for high permeabilities.

The most important conclusion from Figure 5.2 is that the two previously used criteria are not sufficient, while the third criterion is. It is thus recommended to adopt the third criterion in the velocity-based 2-phase formulation.

It should be noted that the third criterion can be used as an estimate for the critical time step size in calculations involving more than one dimension. It requires substitution of Δx_0 by the characteristic length of an element. In three dimensions the tetrahedral element is a popular choice. Its characteristic length is given by the minimum altitude of the tetrahedral element, which is given by the shortest distance between the side of maximum area and the opposite vertex [22].

6

MATERIAL POINT METHOD

To mitigate the problem of element distortion that can occur with analyses of large deformation processes with the FEM, the material point method has been introduced by Sulsky [17]. It uses a cloud of material points to discretize a solid body. The deformation of the solid, e.g. soil, is simulated by tracking the movement of the material points through a fixed background mesh. Incremental movements of material points are computed by first solving the momentum equations at nodes of the background mesh and then mapping the nodal velocities and corresponding displacements to the material points. Because the calculation steps of the MPM are to a large extent identical to those of FEM, MPM can be considered as an extension of the former.

In this chapter the application of the obtained stability criterion with the MPM is considered. First, a brief introduction to the material point method is presented. The discretization and initialization are described in Section 6.1 and the solution procedure in Section 6.2. Finally, the application of the finite element stability criterion is presented in Section 6.3.

6.1. DISCRETIZATION AND INITIALIZATION

Material points represent subvolumes of a solid body. They are placed inside the finite elements of the background mesh according to the initial configuration of the solid body, see Figure 6.1. In order to accomodate for the arbitrary large deformations of the solid body, the finite element mesh must cover the entire region of space that the solid body is expected to move. As material points move through the mesh, initially empty elements might become filled with material points, while full elements become empty. Nodes are called inactive if all adjacent elements are empty, otherwise they are called active.

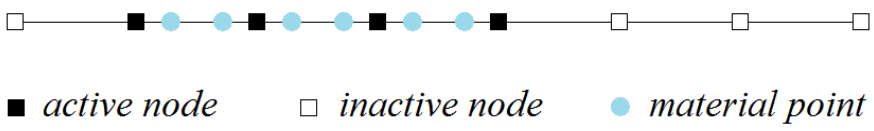

Figure 6.1: MPM discretization in one dimension

It might be assumed that the material points initially cover the volumes of occupied elements entirely. Each material point p in element e with n_{ep} material points then represents an equal portion of the element volume V_e, being

$$V_p = \frac{V_e}{n_{ep}}. \tag{6.1}$$

In one dimension, this is equivalent to

$$\Delta x_p = \frac{\Delta x_e}{n_{ep}}, \tag{6.2}$$

when letting the dimensions in the transverse directions be unit length.

Material points carry all information of the subvolumes of the solid body they represent, such as mass, velocity and stress, as well as possible loads. In addition to the global position x_p and local position ξ_p, these and other state parameters are initially assigned to each material point.

6.2. SOLUTION PROCEDURE

At the beginning of a time step n, the global mass matrices and force vectors of the 2-phase formulation (Equation 4.21 to 4.30) are constructed as with FEM. Here, the material points take over the function of Gaussian integration points. The element mass matrix in the momentum equation for water is for example given by

$$\mathbf{M}^n_{w,e} = \sum_{p=1}^{n_{ep}} \rho^n_{w,p} \Delta x^n_p \mathbf{N}^T_{ep} \mathbf{N}_{ep}, \tag{6.3}$$

with $\mathbf{N}_{ep} = \mathbf{N}_e(\xi_p)$ being the element shape function vector calculated at the position of material point p.

Nodal velocities are initialized through a mass weighted mapping of material point velocities that is consistent with the mapping of linear momentum $\mathbf{P}^n$. We distinguish of course between the velocities of the soil and the water phase

$$\mathbf{v}^n_w = \left(\bar{\mathbf{M}}^n_w\right)^{-1} \mathbf{P}^n_w \qquad \text{with} \qquad \mathbf{P}^n_{w,e} = \sum_{p=1}^{n_{ep}} n \rho^n_w \Delta x^n_p \mathbf{N}^T_{ep} v^n_{w,p}, \tag{6.4}$$

$$\mathbf{v}^n_s = \left(\mathbf{M}^n_s\right)^{-1} \mathbf{P}^n_s \qquad \text{with} \qquad \mathbf{P}^n_{s,e} = \sum_{p=1}^{n_{ep}} (1-n) \rho^n_s \Delta x^n_p \mathbf{N}^T_{ep} v^n_{s,p}. \tag{6.5}$$

Identical to the finite element implementation presented in Chapter 4, the Euler-Cromer scheme is applied to the 2-phase formulation. This means that the velocities are updated explicitly and the effective stress and pore pressure implicitly.

First nodal accelerations of both phases are computed

$$\mathbf{a}^n_w = \left(\mathbf{M}^n_w\right)^{-1} \left(\mathbf{F}^{trac,w} - \mathbf{F}^{int,w} + \mathbf{F}^{grav,w} - \mathbf{F}^{drag,w}\right), \tag{6.6}$$

$$\mathbf{a}^n_s = \left(\mathbf{M}^n_s\right)^{-1} \left(-\bar{\mathbf{M}}^n_w \mathbf{a}^n_w + \mathbf{F}^{trac} - \mathbf{F}^{int} + \mathbf{F}^{grav}\right). \tag{6.7}$$

It should be noted that nodes might get a small mass assigned when a single material point enters an initially empty element and the material point is still close to the element boundary, so that the mass matrices might become nearly singular. This can subsequently lead to unrealistically high nodal accelerations. When the nodal velocities are directly updated from the nodal accelerations, they can become unrealistically high as well.

A remedy proposed by Sulsky [31] is to first update the velocities of the material points using the nodal accelerations

$$v_{w,p}^{n+1} = v_{w,p}^{n} + \Delta t \mathbf{N}_{ep} \mathbf{a}_{w,e}^{n}, \tag{6.8}$$

$$v_{s,p}^{n+1} = v_{s,p}^{n} + \Delta t \mathbf{N}_{ep} \mathbf{a}_{s,e}^{n}. \tag{6.9}$$

Then, nodal velocities are updated as in Equation 6.6 and 6.7

$$\mathbf{v}_{w}^{n+1} = \left(\bar{\mathbf{M}}_{w}^{n}\right)^{-1} \mathbf{P}_{w}^{n+1}, \tag{6.10}$$

$$\mathbf{v}_{s}^{n+1} = \left(\mathbf{M}_{s}^{n}\right)^{-1} \mathbf{P}_{s}^{n+1}. \tag{6.11}$$

The pore pressure and the effective stress at the material points are computed implicitly by

$$p_{p}^{n+1} = p^{n} + \Delta t \left[\mathbf{K}_{ep}^{s,n} \mathbf{v}_{s,e}^{n+1} + \mathbf{K}_{ep}^{w,n} \mathbf{v}_{w,e}^{n+1}\right], \tag{6.12}$$

$$\sigma'^{\,n+1}_{p} = \sigma'^{\,n}_{p} + \Delta t \left[\bar{\mathbf{K}}_{ep}^{s,n} \mathbf{v}_{s,e}^{n+1}\right]. \tag{6.13}$$

It should be noted that element matrices in Equation 6.12 and 6.13 are constructed based on the slope of the shape functions and the step functions at material point p.

$$\mathbf{LN}_{ep}^{n} = \left[-\frac{1}{\Delta x_0} \quad \frac{1}{\Delta x_0}\right], \tag{6.14}$$

$$\mathbf{K}_{ep}^{n} = \left[1\right]. \tag{6.15}$$

Finally, the global positions of the material points are updated from the incremental nodal displacements $\Delta \mathbf{u}_{s}^{n+1} = \Delta t \mathbf{v}_{s}^{n+1}$. Material points crossing element boundaries are assigned to new elements.

The solution procedure is repeated for a successive time step.

6.3. NUMERICAL STABILITY

With FEM, each element represents a subvolume of the solid body. Based on the material properties of this subvolume stored at the Gauss point, the critical time step size can be approximated with the heuristic estimate $\Delta t_{crit,3}$ obtained in Section 5.3.

With MPM, the critical time step size is also determined by the finite element calculation. However, an element no longer has fixed material properties, since they depend on the number of material points that is inside the element and the material properties belonging to these material points. Owing to the material points crossing element boundaries they might change during the calculation. It is therefore recommended to recalculate the critical time step size at the end of each time step.

The calculation of critical time step size $\Delta t_{crit,3}$ is done for all elements and all material points within them. The calculation of the critical time step size for material point p in element e is given by

$$\Delta t_{crit,3,p} = \frac{-2a + \sqrt{4a^2 + 8\left(b + \sqrt{b^2 - 4d}\right)}}{b + \sqrt{b^2 - 4d}}. \tag{6.16}$$

with coefficients

$$a = \frac{n\rho_{sat} g}{(1-n)\rho_s k}, \tag{6.17}$$

$$b = \frac{4\left(n\rho_{sat} K_w + (1-2n)\rho_w K_w + n\rho_w E^c\right)}{n(1-n)\rho_s \rho_w \Delta x_0^2}, \tag{6.18}$$

$$d = \frac{16 E^c K_w}{(1-n)\rho_s \rho_w \Delta x_0^4}. \tag{6.19}$$

Here, the material properties n, ρ_s, ρ_w, k, E^c and K_w stored at the material point and the element size Δx_0 of the parent element are used.

The minimum critical time step size is used to update the time step size

$$\Delta t_{crit,3} = \min_e \min_p \Delta t_{crit,3,p}. \tag{6.20}$$

The mass weighted mapping of data from the material points to the nodes and back is expected to influences the critical time step size. This influence is difficult to capture in an expression. However, it is expected to cause some relaxation of the critical time step size, such that the MPM is stable for $\Delta t > \Delta t_{crit,3}$. Analyses confirm this expectation.

7

CONCLUDING REMARKS

In this thesis, the numerical stability of the velocity-based 2-phase formulation has been studied; i.e. the dependency of the critical time step size of the considered Euler-Cromer time integration scheme on the permeability, the stiffness of the soil and pore water, as well as the minimum element size.

While the task was to obtain a time step criterion for the material point method (MPM), the finite element method (FEM) has been mainly considered to simplify this demanding task. However, because the MPM can be considered as an extension of FEM, results can be readily transferred to the MPM.

The frame conditions for the study are given by the MPM code developed by Deltares and partners: a homogeneous and isotropic continuum is considered. The soil is modelled as linear-elastic, the pore water as linearly compressible. Linear shape functions, Gaussian quadrature and lumped matrices are used in the numerical framework.

The stability analyses of the velocity-based 2-phase formulation performed in this thesis resulted in three estimates for the critical time step size. Two estimates were obtained from two variants of the matrix method. The third estimate is a heuristic combination of both, given by

$$\Delta t_{crit,3} = \frac{-2a + \sqrt{4a^2 + 8\left(b + \sqrt{b^2 - 4d}\right)}}{b + \sqrt{b^2 - 4d}},$$

with coefficients

$$a = \frac{n\rho_{sat} g}{(1-n)\rho_s k},$$

$$b = \frac{4\left(n\rho_{sat} K_w + (1-2n)\rho_w K_w + n\rho_w E^c\right)}{n(1-n)\rho_w \rho_s \Delta x_0^2},$$

$$d = \frac{16 E^c K_w}{(1-n)\rho_w \rho_s \Delta x_0^4}.$$

With the help of a benchmark of one-dimensional wave propagation, it was concluded that this third estimate renders the most reliable, yet efficient solution. To the author's knowledge, it is the first sufficient criterion for the velocity-based 2-phase formulation. It renders a significant improvement compared to the criteria available so far: the mesh-dependent CFL condition for undrained wave propagation and the permeability-dependent criterion obtained during the preliminary study of this thesis. It allows for robust and efficient numerical analyses of dynamic geotechnical problems with the 2-phase FEM and MPM.

If material properties and/or element sizes change during a computation, the time step size must be adapted to a newly computed critical time step size. In this way results also apply to analyses involving geometric and material non-linearity. An extension of the criterion to two or three dimensions would seem easily possible. It requires computation of a characteristic length of an element, which replaces the parameter Δx_0, the length of a line element.

With regard to MPM, the obtained stability criterion is recommended to be applied to each material point in combination with the characteristic length of the parent element. Since material points cross element boundaries, the critical time step size must be recomputed after each time step.

Through the extensive study in this thesis, new insight has been gained into the numerical stability of the velocity-based 2-phase formulation. However, the influence of techniques used with the considered MPM code, such as strain smoothening and (local) damping, was not addressed and requires more research. Another interesting subject of research would be permeability scaling next to mass scaling, such that quasi-static problems with a low permeability converge faster to their equilibrium. Adjustment of the time integration scheme could be investigated to allow for larger time step sizes.

A

PHYSICAL MODEL IN THREE DIMENSIONS

This appendix will extend the velocity-based 2-phase formulation presented in Chapter 3 to three dimensions by pointing out the differences between one and three dimensions. Following the outline of Chapter 3, the relevant variables are defined first. Then, the equations corresponding to conservation of mass and conservation of momentum are presented, as well as the constitutive relation. Finally, the initial and boundary conditions are addressed.

DEFINITION OF VARIABLES

The deformation of saturated soil is presented in terms of the velocity of the soil, the velocity of the water, the effective stress and the pore pressure. The increase of the number of dimensions does not affect the number of variables, but it does change the shape of the variables.

The displacement and velocity of both soil and water are now vector functions with three components

$$\hat{\mathbf{u}}_s(\mathbf{x}_0,t) = \begin{bmatrix} \hat{u}_{s,1}(\mathbf{x}_0,t) \\ \hat{u}_{s,2}(\mathbf{x}_0,t) \\ \hat{u}_{s,3}(\mathbf{x}_0,t) \end{bmatrix}, \qquad \hat{\mathbf{u}}_w(\mathbf{x}_0,t) = \begin{bmatrix} \hat{u}_{w,1}(\mathbf{x}_0,t) \\ \hat{u}_{w,2}(\mathbf{x}_0,t) \\ \hat{u}_{w,3}(\mathbf{x}_0,t) \end{bmatrix}, \tag{A.1}$$

$$\hat{\mathbf{v}}_s(\mathbf{x}_0,t) = \begin{bmatrix} \hat{v}_{s,1}(\mathbf{x}_0,t) \\ \hat{v}_{s,2}(\mathbf{x}_0,t) \\ \hat{v}_{s,3}(\mathbf{x}_0,t) \end{bmatrix}, \qquad \hat{\mathbf{v}}_w(\mathbf{x}_0,t) = \begin{bmatrix} \hat{v}_{w,1}(\mathbf{x}_0,t) \\ \hat{v}_{w,2}(\mathbf{x}_0,t) \\ \hat{v}_{w,3}(\mathbf{x}_0,t) \end{bmatrix}, \tag{A.2}$$

continuously depending on material coordinates $\mathbf{x}_0 = \begin{bmatrix} x_{0,1} & x_{0,2} & x_{0,3} \end{bmatrix}^T$ and time t.

The total stress and effective stress in the soil become second order tensors with normal stress on the diagonal and shear stress off the diagonal, denoted by

$$\hat{\sigma}_{ij}(\mathbf{x}_0,t) = \begin{bmatrix} \sigma_{11} & \sigma_{12} & \sigma_{13} \\ \sigma_{21} & \sigma_{22} & \sigma_{23} \\ \sigma_{31} & \sigma_{32} & \sigma_{33} \end{bmatrix}, \qquad \hat{\sigma}'_{ij}(\mathbf{x}_0,t) = \begin{bmatrix} \sigma'_{11} & \sigma'_{12} & \sigma'_{13} \\ \sigma'_{21} & \sigma'_{22} & \sigma'_{23} \\ \sigma'_{31} & \sigma'_{32} & \sigma'_{33} \end{bmatrix}. \tag{A.3}$$

Since the pore pressure, denoted by scalar function $\hat{p}(\mathbf{x}_0, t)$, only affects the normal stress, the principle of effective stress by Terzaghi [10] becomes

$$\hat{\sigma}_{ij}(\mathbf{x}_0, t) = \hat{\sigma}'_{ij}(\mathbf{x}_0, t) + \hat{p}(\mathbf{x}_0, t)\delta_{ij}, \tag{A.4}$$

with δ_{ij} being the Kronecker delta.

CONSERVATION OF MASS

The derivation of the storage equation in three dimensions is similar to the derivation in one dimension. First, the conservation of mass of the soil is expressed as

$$\frac{\partial}{\partial t}\left[(1-n)\rho_s\right] + \frac{\partial}{\partial x_{0,i}}\left[(1-n)\rho_s \hat{v}_{s,i}\right] = 0, \tag{A.5}$$

where we use the Einstein summation convention to denote summation over the three dimensions.

Similarly, the conservation of mass of the water is expressed as

$$\frac{\partial}{\partial t}\left[n\rho_w\right] + \frac{\partial}{\partial x_{0,i}}\left[n\rho_w \hat{v}_{w,i}\right] = 0. \tag{A.6}$$

Assuming incompressible soil and linearly compressible water, see Equation 3.10, and neglecting a spatial variation in density and porosity, we reduce Equation A.5 and A.6 to

$$-\rho_s \frac{\partial n}{\partial t} + (1-n)\rho_s \frac{\partial \hat{v}_{s,i}}{\partial x_{0,i}} = 0, \tag{A.7}$$

$$-\frac{n\rho_w}{K_w}\frac{\partial \hat{p}}{\partial t} + \rho_w \frac{\partial n}{\partial t} + n\rho_w \frac{\partial \hat{v}_{w,i}}{\partial x_{0,i}} = 0. \tag{A.8}$$

Elimination of the term $\frac{\partial n}{\partial t}$ yields the storage equation, being

$$\frac{\partial \hat{p}}{\partial t} = \frac{K_w}{n}\left[(1-n)\frac{\partial \hat{v}_{s,i}}{\partial x_{0,i}} + n\frac{\partial \hat{v}_{w,i}}{\partial x_{0,i}}\right]. \tag{A.9}$$

CONSERVATION OF MOMENTUM

It should be noted that the conservation of angular momentum can not be neglected in three dimensions. Since this only implies that the stress tensors are symmetric, i.e. $\sigma'_{ij} = \sigma'_{ji}$ and $\sigma_{ij} = \sigma_{ji}$, no new equations are required in the considered 2-phase formulation.

The conservation of linear momentum for soil yields

$$(1-n)\rho_s \frac{\partial \hat{v}_{s,i}}{\partial t} = \frac{\partial \hat{\sigma}'_{ij}}{\partial x_{0,j}} + (1-n)\frac{\partial \hat{p}}{\partial x_{0,i}} + (1-n)\rho_s g_i + \frac{n^2 \rho_w g}{k}(\hat{v}_{w,i} - \hat{v}_{s,i}). \tag{A.10}$$

Here, the internal forces are composed of the normal stress, shear stress and pore pressure. The gravitational acceleration is given by the vector $\mathbf{g} = \begin{bmatrix} 0 & -g & 0 \end{bmatrix}^T$, assuming that the second dimension denotes the vertical direction.

The conservation of linear momentum for the water phase is given by

$$n\rho_w \frac{\partial \hat{v}_{w,i}}{\partial t} = n\frac{\partial \hat{p}}{\partial x_{0,i}} + n\rho_w g_i - \frac{n^2 \rho_w g}{k}(\hat{v}_{w,i} - \hat{v}_{s,i}). \tag{A.11}$$

The conservation of linear momentum of the soil-water mixture is obtained by the sum of Equation A.10 and A.11, yielding

$$(1-n)\rho_s \frac{\partial \hat{v}_{s,i}}{\partial t} + n\rho_w \frac{\partial \hat{v}_{w,i}}{\partial t} = \frac{\partial \hat{\sigma}'_{ij}}{\partial x_{0,j}} + \frac{\partial \hat{p}}{\partial x_{0,i}} + \rho_{sat} g_i. \tag{A.12}$$

Constitutive relation

In three dimensions, the constitutive relation for an isotropic linear-elastic material is given by Hooke's law

$$\frac{\partial \hat{\sigma}'_{ij}}{\partial t} = D_{ijkl} \frac{\partial \hat{v}_k}{\partial x_{0,l}}, \tag{A.13}$$

with D_{ijkl} being the constitutive tensor

$$D_{ijkl} = (K - \frac{2}{3}G)\delta_{ij}\delta_{kl} + G(\delta_{ik}\delta_{jl} + \delta_{il}\delta_{jk}). \tag{A.14}$$

Here, K and G represent the bulk modulus and the shear modulus of the soil, respectively. They are related to Young's modulus E and Poisson ratio ν by

$$K = \frac{E}{3(1-2\nu)} \qquad \text{and} \qquad G = \frac{E}{2(1+\nu)}. \tag{A.15}$$

Initial and boundary conditions

The equations considered in the velocity-based 2-phase formulation form a system of coupled partial differential equations that should be satisfied on a certain three-dimensional domain Ω. In order for the 2-phase formulation to have a unique solution, one boundary condition is required for each phase at each point of the boundary $\partial\Omega$.

We consider both Dirichlet boundary conditions and Neumann boundary conditions. For the soil phase this results in the prescribed velocity boundary $\partial\Omega_s$ and the prescribed total stress boundary $\partial\Omega_\sigma$. For the water phase we distinguish between the prescribed velocity boundary $\partial\Omega_w$ and the prescribed pressure boundary $\partial\Omega_p$. Similar to the one-dimensional case, we have intersection and union criteria

$$\partial\Omega_s \cap \partial\Omega_\sigma = \emptyset, \qquad \partial\Omega_s \cup \partial\Omega_\sigma = \partial\Omega, \tag{A.16}$$

$$\partial\Omega_w \cap \partial\Omega_p = \emptyset, \qquad \partial\Omega_w \cup \partial\Omega_p = \partial\Omega. \tag{A.17}$$

The velocity boundary conditions are written as

$$\hat{v}_{s,i}(\mathbf{x}_0, t) = \bar{v}_{s,i}(\mathbf{x}_0, t) \quad \text{on } \partial\Omega_s, \tag{A.18}$$
$$\hat{v}_{w,i}(\mathbf{x}_0, t) = \bar{v}_{w,i}(\mathbf{x}_0, t) \quad \text{on } \partial\Omega_w. \tag{A.19}$$

The total traction and pressure boundary conditions are written as

$$\hat{\sigma}_{ij}(\mathbf{x}_0, t) n_j = \bar{\sigma}_i(\mathbf{x}_0, t) \quad \text{on } \partial\Omega_\sigma, \tag{A.20}$$
$$\hat{p}(\mathbf{x}_0, t) n_i = \bar{p}_i(\mathbf{x}_0, t) \quad \text{on } \partial\Omega_p. \tag{A.21}$$

Here, n_j denotes the j-th component of the unit normal vector.

Since the system of partial differential equations is first order in time, one initial condition is necessary for each variable

$$\hat{v}_{s,i}(\mathbf{x}_0, 0) = \bar{v}_{s,i,0}(\mathbf{x}_0), \tag{A.22}$$
$$\hat{v}_{w,i}(\mathbf{x}_0, 0) = \bar{v}_{w,i,0}(\mathbf{x}_0), \tag{A.23}$$
$$\hat{\sigma}'_{ij}(\mathbf{x}_0, 0) = \bar{\sigma}'_{ij,0}(\mathbf{x}_0), \tag{A.24}$$
$$\hat{p}(\mathbf{x}_0, 0) = \bar{p}_0(\mathbf{x}_0). \tag{A.25}$$

B

COORDINATE TRANSFORMATION

In the frame of this thesis, a transformation is considered from a global coordinate system to a local coordinate system. Let x_0 be the coordinate of the one-dimensional global coordinate system, in which an element is bounded by x_i and x_{i+1}. The coordinate ξ of the local element coordinate system is bounded by 0 and 1. The transformation is illustrated in Figure B.1 and mathematically written as

$$x_0 = (1-\xi)x_i + \xi x_{i+1} = x_i + (x_{i+1} - x_i)\xi. \tag{B.1}$$

It should be noted that the coordinate transformation is characterized by the Jacobian J, being

$$J = \frac{dx_0}{d\xi} = x_{i+1} - x_i. \tag{B.2}$$

The Jacobian appears with the transformation of derivatives and integrals.

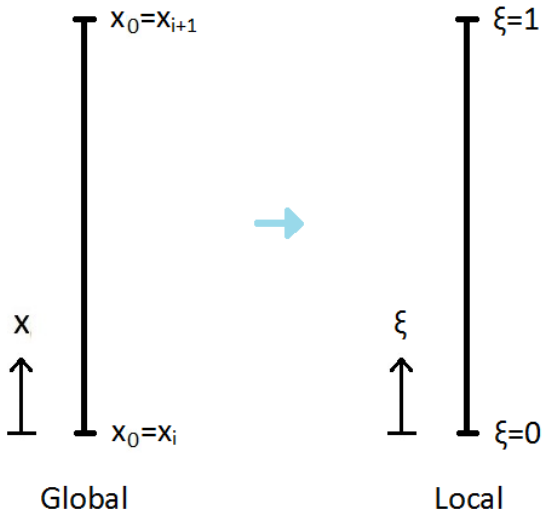

Figure B.1: Global and local coordinate system [9]

C

GAUSSIAN QUADRATURE

Gaussian quadrature is a method to numerically approximate a definite integral as a weighted sum of function values at so-called Gauss points. An n-point Gaussian quadrature rule uses n Gauss points and is by definition exact for polynomials up to order $2n-1$.

In order to explain Gaussian quadrature, an integral of a function $g(x)$ over a line segment $[a,b]$ is considered, as illustrated in Figure C.1. The n-point Gaussian quadrature rule approximates the integral by

$$\int_a^b g(x)dx \approx \sum_{q=1}^{n} \omega_q g(x_q), \tag{C.1}$$

with weight ω_q and position x_q for each Gauss point q.

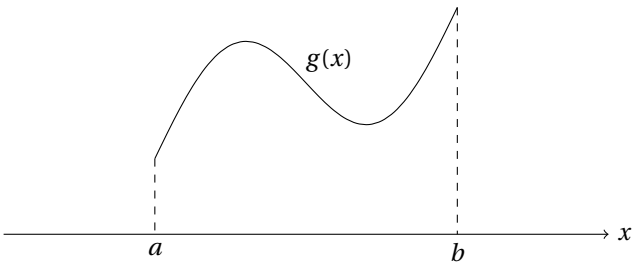

Figure C.1: Function $g(x)$ at line segment $[a,b]$

In case of a single Gauss point, we calculate its weight ω_q and coordinate x_q by defining that Gaussian quadrature is exact for polynomials up to order one

$$\int_a^b dx = b-a = \omega_q \rightarrow \omega_q = b-a, \tag{C.2}$$

$$\int_a^b x dx = \frac{1}{2}(b^2-a^2) = \omega_q x_q \rightarrow x_q = \frac{1}{2}(b+a). \tag{C.3}$$

From Equation C.2 and C.3 it is concluded that the location of the Gauss point is exactly in the middle of the line segment. The weight equals the length of the line segment.

D

ASSEMBLAGE PROCEDURE

The finite element method is considered to be an attractive numerical method for space discretization, because of the convenient assemblage of global matrices from element matrices. This appendix explains an assemblage procedure that is described by Loghin [32].

For a global matrix $\mathbf{M}$ and corresponding element matrices $\mathbf{M}_e$ the assemblage procedure is written as

$$\mathbf{M} = \sum_{e=1}^{n_e} \mathbf{A}_e^T \mathbf{M}_e \mathbf{A}_e, \tag{D.1}$$

with matrix $\mathbf{A}_e$ being a boolean matrix representing the mapping between global and local node numbers of element e.

As an example, we consider the three line elements in Figure D.1.

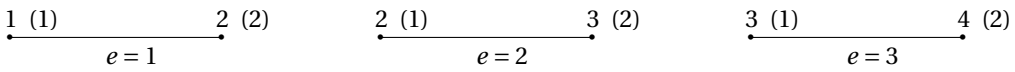

Figure D.1: Three line elements with global and local node numbers

From the global and local node numbers we can derive the boolean matrices $\mathbf{A}_e$, being

$$\mathbf{A}_1 = \begin{bmatrix} 1 & 0 & 0 & 0 \\ 0 & 1 & 0 & 0 \end{bmatrix}, \quad \mathbf{A}_2 = \begin{bmatrix} 0 & 1 & 0 & 0 \\ 0 & 0 & 1 & 0 \end{bmatrix}, \quad \mathbf{A}_3 = \begin{bmatrix} 0 & 0 & 1 & 0 \\ 0 & 0 & 0 & 1 \end{bmatrix}. \tag{D.2}$$

When the element matrices $\mathbf{M}_e$ equal

$$\mathbf{M}_1 = \begin{bmatrix} 1 & 1 \\ 1 & 1 \end{bmatrix}, \quad \mathbf{M}_2 = \begin{bmatrix} 2 & 2 \\ 2 & 2 \end{bmatrix}, \quad \mathbf{M}_3 = \begin{bmatrix} 3 & 3 \\ 3 & 3 \end{bmatrix}, \tag{D.3}$$

the global matrix $\mathbf{M}$ is constructed with the assemblage procedure to be

$$\mathbf{M} = \begin{bmatrix} 1 & 1 & 0 & 0 \\ 1 & 3 & 2 & 0 \\ 0 & 2 & 5 & 3 \\ 0 & 0 & 3 & 3 \end{bmatrix}. \tag{D.4}$$

E

LUMPING PROCEDURE

With the lumping procedure a diagonal matrix is constructed from a non-diagonal matrix. The diagonal and the non-diagonal matrix are denoted as the lumped matrix $\mathbf{A}^L$ and the full matrix $\mathbf{A}$, respectively. Each diagonal entry of the lumped matrix equals the row sum of the full matrix

$$\mathbf{A}^L_{ii} = \sum_{j=1}^{n} A_{ij}. \tag{E.1}$$

Consider for example the following full matrix

$$\mathbf{A} = \begin{bmatrix} 4 & 0 & 1 & 1 \\ 2 & 9 & 1 & 0 \\ 0 & 1 & 3 & 0 \\ 1 & 2 & 0 & 5 \end{bmatrix}. \tag{E.2}$$

Applying the lumping procedure to $\mathbf{A}$ results in the lumped matrix

$$\mathbf{A}^L = \begin{bmatrix} 6 & 0 & 0 & 0 \\ 0 & 12 & 0 & 0 \\ 0 & 0 & 4 & 0 \\ 0 & 0 & 0 & 8 \end{bmatrix}. \tag{E.3}$$

BIBLIOGRAPHY

[1] A. Elgamal, E. Parra, Z. Yang, and K. Adalier, *Numerical analysis of embankment foundation liquefaction countermeasures,* Journal of Earthquake Engineering **6**, p. 447 (2002).

[2] F. Ceccato, A. Rohe, and P. Simonini, *Simulation of slope failure experiment with the material point method,* in *Incontro Annuale Ricercatori di Geotecnica* (2014).

[3] Z. Cheng and B. Jeremić, *Numerical modeling and simulation of pile in liquefiable soil,* Soil Dynamics and Earthquake Engineering **29**, p. 1405 (2009).

[4] J. M. Huyghe, D. H. van Campen, T. Arts, and R. M. Heethaar, *A two-phase finite element model of the diastolic left ventricle,* Journal of Biomechanics **24**, p. 527 (1991).

[5] S. L. Butler, S. S. Kohles, R. J. Thielke, C. Chen, and R. Vanderby Jr, *Interstitial fluid flow in tendons or ligaments: a porous medium finite element simulation,* Medical and Biological Engineering and Computing **35**, p. 742 (1997).

[6] T. G. Zieliński, *Numerical investigation of active porous composites with enhanced acoustic absorption,* Journal of Sound and Vibration **330**, p. 5292 (2011).

[7] F. Ceccato, *Study of large deformation geomechanical problems with the material point method,* Ph.D. thesis, Università degli studi di Padova (2015).

[8] R. Courant, K. Friedrichs, and H. Lewy, *Über die partiellen Differenzengleichungen der mathematischen Physik,* Mathematische Annalen **100**, p. 32 (1928).

[9] M. M. J. Mieremet, *Numerical stability for velocity-based 2-phase formulation for geotechnical dynamic analysis,* Technical Report 15-3 (Delft Institute of Applied Mathematics, 2015).

[10] K. von Terzaghi, *Erdbaumechanik auf bodenphysikalischer Grundlage* (Deuticke, 1925).

[11] M. Biot, *General theory of three-dimensional consolidation,* Journal of Applied Physics **12**, p. 155 (1941).

[12] O. Zienkiewicz, A. Chan, M. Pastor, B. Schrefler, and T. Shiomi, *Computational geomechanics with special reference to earthquake engineering* (John Wiley, 1999).

[13] L. Xikui and O. Zienkiewicz, *Multiphase flow in deforming porous media and finite element solutions,* Computers & Structures **45**, p. 211 (1992).

[14] A. Yerro, E. Alonso, and N. Pinyol, *The material point method for unsaturated soils,* Géotechnique **65**, p. 201 (2015).

[15] H.-S. Yu, *Plasticity and geotechnics* (Springer, 2006).

[16] J. v. Kan, A. Segal, and F. Vermolen, *Numerical methods in scientific computing* (VSSD, 2008).

[17] D. Sulsky, Z. Chen, and H. L. Schreyer, *A particle method for history-dependent materials,* Computer Methods in Applied Mechanics and Engineering **118**, p. 179 (1994).

[18] A. Cromer, *Stable solutions using the Euler approximation,* American Journal of Physics **49**, p. 455 (1981).

[19] J. E. Guilkey and J. Weiss, *Implicit time integration for the material point method: Quantitative and algorithmic comparisons with the finite element method,* International Journal for Numerical Methods in Engineering **57**, p. 1323 (2003).

[20] D. Sulsky and A. Kaul, *Implicit dynamics in the material-point method,* Computer Methods in Applied Mechanics and Engineering **193**, p. 1137 (2004).

[21] J. Van Esch, D. Stolle, and I. Jassim, *Finite Element Method for Coupled Dynamic Flow-Deformation Simulation,* in *2nd International Symposium on Computational Geomechanics* (2011).

[22] I. AL-Kafaji, *Formulation of a dynamic material point method (MPM) for geomechanical problems*, Ph.D. thesis, Institut für Geotechnik der Universität Stuttgart (2013).

[23] L. Malvern, *Introduction to the Mechanics of a Continuous Medium* (Prentice Hall, 1969).

[24] A. Verruijt, *An introduction to soil dynamics* (Springer, 2010).

[25] C. Hirsch, *Numerical computation of internal and external flows: the fundamentals of numerical discretization* (John Wiley & Sons, 1988).

[26] B. Irons and S. Ahmad, *Techniques of finite elements* (Ellis Horwood, 1980).

[27] S. L. Shmakov, *A universal method of solving quartic equations,* International Journal of Pure and Applied Mathematics **71**, p. 251 (2011).

[28] J. Hoffman, *Numerical methods for engineers and scientists* (McGraw-Hill, 1992).

[29] A. Yerro, *Minimum time step criterion of 2-phase calculation,* presentation at MPM workshop, Barcelona, Spain (June 5, 2015).

[30] M. Mieremet, D. Stolle, F. Ceccato, and C. Vuik, *Numerical stability for modelling of dynamic two-phase interaction,* submitted for publication (2015).

[31] D. Sulsky, S.-J. Zhou, and H. L. Schreyer, *Application of a particle-in-cell method to solid mechanics,* Computer Physics Communications **87**, p. 236 (1995).

[32] D. Loghin, M. van Gijzen, and E. Jonkers, *Bounds on the eigenvalue range and on the field of values of non-Hermitian and indefinite finite element matrices,* Journal of Computational and Applied Mathematics **189**, p. 304 (2006).